tRNA lysidinylation is essential for the minimal translation system found in the apicoplast of *Plasmodium falciparum*

Rubayet Elahi[1,2], Sean T. Prigge[1,2]

[1] Department of Molecular Microbiology and Immunology, Johns Hopkins University, Baltimore, Maryland, USA

[2] The Johns Hopkins Malaria Research Institute, Baltimore, Maryland, USA

Rubayet Elahi

Email: aelahi3@jhu.edu

ORCID ID: 0000-0002-1561-5257

Sean T. Prigge

Email: sprigge2@jhu.edu

ORCID ID: 0000-0001-9684-1733

Abstract

For decades, researchers have sought to define minimal genomes to elucidate the fundamental principles of life and advance biotechnology. tRNAs, essential components of this machinery, decode mRNA codons into amino acids. The apicoplast of malaria parasites encodes 25 tRNA isotypes in its organellar genome - the lowest number found in known translation systems. Efficient translation in such minimal systems depends heavily on post-transcriptional tRNA modifications, especially at the wobble anticodon position. Lysidine modification at the wobble position (C34) of $tRNA_{CAU}$ distinguishes between methionine (AUG) and isoleucine (AUA) codons, altering the amino acid delivered by this tRNA and ensuring accurate protein synthesis. Lysidine is formed by the enzyme tRNA isoleucine lysidine synthetase (TilS) and is nearly ubiquitous in bacteria and essential for cellular viability. We identified a TilS ortholog (*Pf*TilS) located in the apicoplast of *Plasmodium falciparum* parasites. By complementing *Pf*TilS with a bacterial ortholog, we demonstrated that the lysidinylation activity of *Pf*TilS is critical for parasite survival and apicoplast maintenance, likely due to its impact on apicoplast protein translation. Our findings represent the first characterization of TilS in an endosymbiotic organelle, advancing eukaryotic organelle research and our understanding of minimal translational machinery. Due to the absence of lysidine modifications in humans, this research also exposes a potential vulnerability in malaria parasites that could be targeted by antimalarial strategies.

Significance

In recent decades, synthetic biologists have sought the minimal cellular components required for life, focusing on simpler systems for easier modeling. The apicoplast organelle of malaria parasites, with only 25 tRNA isotypes, contains the smallest known complete tRNA set, even smaller than in synthetic organisms. This makes it an ideal model for studying minimal translational machinery, where tRNAs depend on post-transcriptional modifications for efficient protein translation. A key modification, lysidine, is crucial for decoding isoleucine and methionine. This study describes a tRNA-isoleucine lysidine synthetase (TilS) enzyme, essential for apicoplast protein translation. These findings have implications for understanding eukaryotic organelles and minimal translation machinery. Additionally, the absence of lysidine in humans suggests a potential target for antimalarial strategies.

Introduction

Elucidating the minimal genome and its translational machinery is fundamental to understanding life and advancing biotechnology. Central to cellular maintenance is the translational machinery, comprising RNA molecules (tRNA, mRNA, rRNA, and other small RNAs) and associated proteins. Transfer RNAs (tRNAs) are vital for protein translation, decoding mRNA codons into amino acids via precise codon-anticodon interactions within the ribosome (1). A key question in synthetic biology is determining the minimum number of tRNA isotypes required for cellular viability. The synthetic minimal genome organism *Mycoplasma mycoides* JCVI-syn3.0 uses 27 tRNA isotypes (2), while the naturally occurring endosymbiotic bacterium *Candidatus Nasuia deltocephalinicola*, with the smallest known bacterial genome, encodes 28 tRNA isotypes (3). Intriguingly, the apicoplast, an endosymbiotic relict plastid organelle, of *Plasmodium falciparum* contains only 25 tRNA isotypes (4-7), aligning more closely with theoretical predictions for a minimal tRNA set (8). Both theoretical considerations and empirical data suggest that efficient mRNA codon decoding by a minimal tRNA set is facilitated by maximal use of wobble and superwobbling base pairing between the third mRNA codon base (wobble base) and the first tRNA anticodon base (position 34, wobble position), along with post-transcriptional tRNA modifications.

tRNAs undergo extensive post-transcriptional modifications across all kingdoms of life (9). These modifications, particularly at the wobble position of the anticodon, are crucial for fine-tuning wobble base pairing, either promoting or restricting specific interactions. Additionally, modifications at other positions of the anticodon loop (positions 32–38) stabilize tRNA–codon interactions, enhancing translational accuracy. The presence of genes for enzymes involved in anticodon loop modifications, even in smaller bacterial genomes (580-1840 Kb) (3, 10, 11), further underscores the critical role of these modifications for living organisms.

To date, over 30 distinct wobble modifications have been characterized (12). One such modification, lysidine (L or k^2C), is a lysine-containing derivative of cytidine (**Figure 1A**) at the wobble position (C34) of minor isoleucine (Ile) tRNAs with CAU anticodon ($tRNA^{Ile}_{CAU}$) (13-18). The nearly ubiquitous presence of the tRNA-isoleucine lysidine synthetase (TilS) enzyme (**Figure 1B**), responsible for L formation, strongly suggests the near-universal occurrence of this modification across bacterial species (10, 19-23). In its unmodified form, $tRNA^{Ile}_{CAU}$ behaves

similarly to $tRNA^{Met}_{CAU}$, decoding the AUG codon as methionine (Met). However, the introduction of the L34 modification alters the codon specificity of $tRNA^{Ile}_{CAU}$, enabling it to be charged with Ile and decode the AUA codon as Ile. Consequently, this modification results in a shift in both codon and amino acid specificity. The essential role of TilS in accurate translation is evident from the translational defects observed in TilS-deficient *Escherichia coli* (17). Recognizing its importance, the TilS gene was included in the minimal synthetic genome *M. mycoides* JCVI-syn3.0 (2), as well as in all proposed minimal genome concepts to date (10, 24-27).

The complete set of 25 tRNA isotypes in the apicoplast genome of the malaria parasite *P. falciparum* represents, to the best of our knowledge, the minimal tRNA set observed to date, and also aligns with the theoretically proposed minimum tRNA number required for cell viability (8). This makes *P. falciparum* an intriguing model for studying minimal translational machinery. Although the apicoplast encodes all its rRNAs and tRNAs in its genome, it has transferred most of its protein-coding genes, including those for tRNA modification, to the nuclear genome. These proteins are then trafficked back to the organelle via an N-terminal bipartite transit peptide (28). In this work, we identified a TilS ortholog (*Pf*TilS) encoded in the nuclear genome and showed that it is trafficked to the apicoplast organelle. Using an apicoplast metabolic bypass system (29), we showed that *Pf*TilS is essential for apicoplast maintenance and parasite viability. Successful complementation of *Pf*TilS with a characterized bacterial TilS enzyme allowed us to conclude that *Pf*TilS is essential due to its lysidine synthesis activity. To our knowledge, this is the first characterization of TilS in a eukaryote, significantly impacting future eukaryotic organelle research and strengthening our understanding of minimal translational machinery.

Results

Apicomplexan parasite contains a TilS ortholog

Among the 25 apicoplast genome encoded tRNA isotypes, Met and Ile decoding is accomplished with three $tRNA_{CAU}$ (currently annotated as $tRNA^{Met}_{CAU}$) and one $tRNA_{GAU}$ (annotated as $tRNA^{Ile}_{GAU}$) (**Figure 1C**), respectively (5, 7). The $tRNA^{Ile}_{GAU}$ decodes AUU and AUC codons to Ile and $tRNA^{Met}_{CAU}$ decodes AUG as Met. However, there are no annotated $tRNA^{Ile}$ genes to decode AUA codons. In absence of direct evidence of tRNA import into plastid like organelles , it was proposed that $tRNA^{Met}_{CAU}$ can decode AUA codon for Ile with the L34

tRNA modification at the wobble position (7). Intriguingly, AUA is the most frequently used codon for Ile for the 30 proteins encoded in the apicoplast genome (**Figure 1D**). A recent investigation identified 28 distinct tRNA modifications within the total tRNA pool of *P. falciparum* (30). The study did not identify any apicoplast-specific modifications and the authors attributed this to the relatively low contribution of apicoplast RNA (0.5-2% rRNA compared to nuclear-encoded rRNAs) (30). It is likely, however, that modifications like L are made in the apicoplast due to the prokaryotic origin (31-33) of the apicoplast and the predominance of AUA codons in the apicoplast genome. We identified a putative TilS enzyme (PF3D7_0411200) with 28% sequence identity to *Escherichia coli* TilS (*Ec*TilS). This protein is currently annotated as a putative PP-loop family protein (5) and bioinformatic analysis predicts this nuclear-encoded protein to be trafficked to the apicoplast (34). Hereafter, we named this putative protein as *P. falciparum* (*Pf*) TilS.

Multiple sequence alignment (MSA) of the putative *Pf*TilS with TilS orthologs from diverse organisms, including *Synechocystis* sp. (*Sy*TilS), *Aquifex aeolicus* (*Aa*TilS), *Mycoplasma genitalium* (*Mg*TilS), *Ec*TilS, *Geobacillus kaustophilus* (*Gk*TilS), and *Arabidopsis thaliana* (*At*RSY3), revealed the presence of an N-terminal extension of 180 amino acid (aa) residues in *Pf*TilS (**Figure 1E, Supplementary Figure 1**), which is predicted to function as a bipartite transit peptide directing the protein through the secretory system to the apicoplast (34). *Pf*TilS also exhibits conservation in functional domains critical for TilS activity. The protein retains conserved residues responsible for tRNA binding, lysine coordination, and a highly conserved ATP-binding PP-loop motif (SGGXDS) (**Figure 1E, Supplementary Figure 1**) (15, 17). Additionally, *Pf*TilS harbors the TilS-specific domain (TSD) where lysine interacts with the enzyme via hydrophobic interaction (15). The PP-loop motif plays a crucial role in TilS function, activating the C2 position of the target tRNA's cytidine 34 to form an adenylate intermediate in an ATP-dependent manner. Subsequently, the ε-amino group of lysine performs a nucleophilic attack on the C2 position of the adenylate intermediate, resulting in L formation (13-16, 19). Other pathogenic apicoplast-containing apicomplexans also seem to possess nuclear genome encoded TilS orthologs with significant conservation in functional domains and important residues (**Supplementary figure 2**). These observations suggest conservation of AUA decoding in apicoplast-containing apicomplexans. Similar to a type-I TilS protein *Ec*TilS, AlphaFold structural prediction (35, 36) suggests that *Pf*TilS adopts a comparable folding architecture with

three distinct domains: an N-terminal domain (NTD) and two C-terminal domains (CTD1 and CTD2) (**Figure 1F**). Despite similar predicted architecture for *Pf*TilS and *Ec*TilS, maximum likelihood phylogenetic analysis (37) of TilS orthologs shows a relatively distant evolutionary relationship between *P. falciparum* and *E. coli* orthologs (**Supplementary Figure 3**).

Plasmodium falciparum TilS localizes to the apicoplast

To experimentally validate the predicted apicoplast localization of *Pf*TilS, we generated two parasite lines. One line expressed a full-length codon-modified *Pf*TilS (residues 1-1245) fused to three tandem C-terminal V5 epitope tags (designated *pftilS*$^{+}$). The other line expressed a codon-modified N-terminally truncated *Pf*TilS (residues181-1245) fused to a similar V5 tag (designated *trpftilS*$^{+}$) (**Figure 2A**). Both constructs were integrated into the genome of PfMev^{attB} parasites (38) using a knock-in approach mediated by mycobacteriophage integrase-based recombination (39) (**Figure 2B**). Successful generation of both *pftilS*$^{+}$ and *trpftilS*$^{+}$ lines was confirmed by PCR (**Figures 2C**).

Immunofluorescence analysis of *pftilS*$^{+}$ parasites revealed colocalization of V5-tagged *Pf*TilS with the apicoplast marker protein, acyl carrier protein (ACP) (28) (**Figure 2D**). This colocalization validates the predicted apicoplast localization of *Pf*TilS and aligns with previous observations of *Pf*TilS protein within the apicoplast proteome identified by proximity biotinylation-based proteomics (40). Conversely, truncated *Pf*TilS in parasites (*trpftilS*$^{+}$) displayed a diffuse cytosolic localization pattern, as expected for a protein lacking an apicoplast targeting peptide. This localization pattern demonstrates that the N-terminal 180 aa residues of *Pf*TilS are required for apicoplast trafficking.

*Pf*TilS is essential for parasite survival and apicoplast maintenance

We used CRISPR/Cas9 mediated gene deletion (41) to assess *Pf*TilS essentiality in a metabolic bypass parasite line, PfMev^{attB} (**Figure 3A**). PfMev^{attB} parasites contain an engineered metabolic pathway to synthesize the isoprenoid precursors IPP (isopentenyl pyrophosphate) and DMAPP (dimethylallyl pyrophosphate) from mevalonate, allowing parasites to survive loss of the apicoplast organelle and its endogenous isoprenoid pathway (29, 38). Additionally, these parasites also express apicoplast-localized Super Folder Green (api-SFG) (42) allowing fluorescent visualization of the organelle (29, 38).

We confirmed the successful deletion of *pftilS* using genotyping PCR (**Figure 3B**). We previously demonstrated that deletion of certain apicoplast tRNA modification genes leads to apicoplast disruption and loss of the organellar genome (43). To investigate whether *pftilS* deletion resulted in apicoplast genome loss, we attempted to amplify the *sufB* gene from the apicoplast genome of Δ*pftilS* parasites. In Δ*pftilS* parasites, our attempt to amplify *sufB* was unsuccessful (**Figure 3C**), suggesting apicoplast genome loss. Consistent with this finding, Δ*pftilS* parasites displayed the characteristic phenotype of apicoplast organelle disruption (42)-multiple, discrete api-SFG labeled vesicles (44) (**Figure 3D**). As anticipated for parasites with disrupted apicoplasts, Δ*pftilS* parasites exhibited a strict dependence on mevalonate for survival (**Figure 3E**).

Collectively, these results demonstrate that *Pf*TilS is essential for both parasite survival and apicoplast maintenance. Given the predicted role of *Pf*TilS in catalyzing a crucial tRNA modification, its deletion likely disrupts the efficient translation of essential apicoplast-encoded proteins, ultimately leading to apicoplast loss and parasite death.

Escherichia coli TilS can be expressed in the *P. falciparum* apicoplast

*Ec*TilS is the most extensively studied and well-characterized TilS ortholog to date. Partial inactivation of *Ec*TilS led to a decrease in level of the L34 modification and to decoding defects for AUA codons (17). Additionally, detailed biochemical (16, 17, 19) and structural (15, 16) studies of *Ec*TilS have been reported. To elucidate the role of *Pf*TilS, we attempted to complement its activity with *Ec*TilS. We achieved this by integrating the *ectilS* gene into PfMev^{attB} parasites using mycobacteriophage integrase-mediated recombination (39) (**Figure 4A**). Hereafter, we refer to this parasite line as *ectilS*$^{+}$. The *ectilS* expression cassette encodes a conditional localization domain (CLD) at the N-terminus to allow inducible control over protein localization (42). It also incorporates an mCherry tag on the C-terminus for visualization by live-cell fluorescence. Additionally, an aptamer array was included in the 3' untranslated region (UTR) of the gene. The CLD facilitates conditional mislocalization of the tagged protein (42), while the TetR-DOZI system regulates protein expression by controlling mRNA stability (45, 46) (**Figure 4B**).

We confirmed successful generation of the *ectilS*$^{+}$ knock-in line with genotyping PCR (**Figure 4C**) and expression of *Ec*TilS-mCherry fusion protein was confirmed via immunoblot

(**Figure 4D**). These parasites did not display significant growth difference compared to the parental line (two-way ANOVA, Mann-Whitney U test, p = 0.3095), suggesting that *Ec*TilS over expression is not toxic to parasites (**Figure 4E**). Live epifluorescence microscopy revealed apicoplast localization of *Ec*TilS protein in the *ectilS*$^{+}$ line, evidenced by colocalization of mCherry fluorescence with that of the apicoplast marker api-SFG (**Figure 4F**). Collectively, these results demonstrate the successful expression and apicoplast targeting of *Ec*TilS in *P. falciparum.*

Escherichia coli TilS functionally complements *P. falciparum* TilS activity in the apicoplast

To assess whether *Ec*TilS could functionally complement *Pf*TilS, we attempted to delete the endogenous parasite *pftilS* gene in the *ectilS*$^{+}$ parasite line using the same guide RNA and repair plasmids used in **Figure 3**. We hypothesized that successful complementation of *Pf*TilS activity by *Ec*TilS would result in a phenotype similar to parental PfMev^{attB} parasites, with intact apicoplasts and no requirement for mevalonate for growth (**Figure 5A**). In repeated independent transfections, we successfully generated *ectilS*$^{+}$Δ*pftilS* parasite lines (**Figure 5B**). These parasites grew without mevalonate supplementation (**Figure 5C**) and appeared to have intact apicoplasts as assessed by both live-cell imaging (**Figure 5D**) and PCR amplification of the apicoplast-encoded *sufB* gene (**Figure 5E**). Furthermore, these parasites did not show any growth defect compared to parental PfMev^{attB} parasites (two-way ANOVA, Mann-Whitney U test, p = 0.8413) (**Figure 5F**). These findings strongly suggest that *Ec*TilS can complement the function of *Pf*TilS.

To further solidify the evidence for complementation by *Ec*TilS, we next aimed to conditionally knockdown *Ec*TilS expression in the *ectilS*$^{+}$Δ*pftilS* parasite line. This was achieved by using the TetR-DOZI and CLD systems previously described in **Figure 4B**. The TetR-DOZI system allows for inducible control of protein expression by regulating mRNA stability in response to non-toxic small molecule anhydrous tetracycline (aTc) (45, 46). The CLD directs the tagged *Ec*TilS protein to the apicoplast under normal conditions. However, upon addition of the non-toxic small molecule ligand *Shield1*, the tagged protein is redirected to the parasitophorous vacuole (**Figure 5G**) (42). We monitored the growth of *ectilS*$^{+}$Δ*pftilS* parasites under permissive (aTc present, *Shield1* absent) and non-permissive conditions (aTc absent, *Shield1* present) for 8 days. Under the non-permissive condition, the *ectilS*$^{+}$Δ*pftilS* parasites displayed a significant growth defect from day 4 (two-way ANOVA, Sidak-Bonferroni method, p = 0.0011) (**Figure**

5H). Live epifluorescence microscopy on day 4 revealed a disrupted apicoplast phenotype in parasites grown under non-permissive conditions (**Figure 5I**). These results demonstrate that *Ec*TilS function is indispensable for maintaining apicoplast integrity following *Pf*TilS deletion and highlight the importance of TilS activity in apicoplast function and parasite survival.

Discussion

The conservation of enzymes that modify tRNA anticodon loop nucleotides (positions 32-38) in nearly all bacteria underscores the critical role that these modifications play in ensuring accurate and efficient protein translation in prokaryotes. Comparative genomic analyses of organisms with reduced genomes consistently identify tRNA modification enzymes targeting the anticodon loop as essential components of minimal translational systems (2, 10, 24-27). TilS, the only known enzyme catalyzing lysidine modification at the anticodon wobble position of $tRNA^{Ile}_{CAU}$, exemplifies this. Lysidine enables precise AUA codon recognition for isoleucine incorporation while preventing AUG codon misreading, thereby dictating both codon specificity and amino acid assignment for $tRNA^{Ile}_{CAU}$. In this work, we took advantage of unique features of apicoplast biology to characterize the first eukaryotic TilS enzyme and show that it is essential for apicoplast maintenance and parasite survival.

The apicoplast (a relict plastid) of the apicomplexan parasite *P. falciparum* has an endosymbiotic origin and encodes a minimal set of 25 complete tRNA isotypes within its circular genome (4-7). This number is lower than the synthetic minimal genome organism *M. mycoides* JCVI-syn3.0, which contains 27 tRNA isotypes (2), positioning the apicoplast as a natural model for studying minimal translational machinery. Another attractive feature of the apicoplast is the ability to delete essential proteins in a metabolic bypass parasite line ($PfMev^{attB}$) that allows the parasites to produce essential isoprenoid products in the cytosol without relying on apicoplast metabolism (29) . In this study, we identified a potential TilS enzyme (*Pf* TilS) encoded in the nuclear genome and used mevalonate supplementation in the $PfMev^{attB}$ line to show that *Pf* TilS is essential for parasite survival (**Figure 3**). The Δ*pftilS* line displayed a 'disrupted apicoplast' phenotype, including loss of the apicoplast genome and the appearance of multiple vesicles containing nucleus-encoded apicoplast proteins. This phenotype was observed in $PfMev^{attB}$ parasites when proteins required for apicoplast maintenance were deleted (43, 47). Importantly,

this was the phenotype observed when the only essential apicoplast tRNA modifying enzyme described (MnmA) to date was deleted (43).

We used a complementation approach to establish the essential function of *Pf* TilS. Biochemical and genetic analyses show that the TilS ortholog from *E. coli* (*Ec*TilS) catalyzes the formation of lysidine on $tRNA^{Ile}_{CAU}$ (16, 17, 19). We found that *Ec*TilS successfully complemented the loss of *Pf* TilS, resulting in parasites with intact apicoplasts. Subsequent knockdown of the complemented *Ec*TilS caused apicoplast disruption, highlighting the essentiality of TilS lysidinylation activity for both apicoplast maintenance and parasite survival (**Figure 5**). These findings strongly suggest that *Plasmodium* TilS catalyzes the lysidinylation of $tRNA_{CAU}$ within the apicoplast. Disruption of tRNA lysidinylation likely disrupts the proper decoding of the most frequently used isoleucine codon (AUA) in apicoplast genome-encoded proteins. Consequently, this would hinder the translation of essential apicoplast proteins, ultimately leading to organelle dysfunction and loss (**Figure 6**).

Although our complementation assays offer robust support for the lysidinylation activity of *Pf*TilS, the L modification in apicoplast-encoded $tRNA_{CAU}$ has not yet been directly observed. Unfortunately, apicoplast disruption and subsequent loss of its genome upon TilS depletion (knockout or knockdown) preclude the investigation of any ribonucleoside modifications within apicoplast tRNAs. Additionally, a recent study surveying the epitranscriptome of *P. falciparum* did not detect ribonucleoside modifications from apicoplast tRNAs. This is likely due to the minor contribution of apicoplast tRNAs to the total parasite tRNA pool, potentially falling below the detection threshold of the employed methodology (30). Future studies using selective enrichment techniques to isolate apicoplast tRNAs, coupled with the inclusion of synthetic standards, offer a promising approach to directly observe the L modification in apicoplast-encoded $tRNA_{CAU}$. Interestingly, the identification of TilS orthologs in chloroplast genomes (48) or in plant nuclear genomes with predicted chloroplast localization (49, 50) suggests a conserved mechanism for isoleucine decoding within diverse plastid organelles. Despite the potential presence of TilS enzymes in other eukaryotic organelles, these enzymes have not been yet characterized, nor have L modifications been reported in organellar $tRNA^{Ile}_{CAU}$ to date (51).

The *P. falciparum* apicoplast genome contains three CAU anticodon bearing tRNAs and all are annotated as $tRNA^{Met}_{CAU}$. This seems to be the case for other major apicoplast containing

pathogenic apicomplexans also (4, 5, 48, 52-56). This raises the possibility that one of the three apicoplast-encoded $tRNA^{Met}_{CAU}$ isoacceptors in *P. falciparum* might be misannotated. In the archaeon *Haloarcula marismortui*, both bioinformatic and biochemical data demonstrated the misannotation of a CAU anticodon-bearing tRNA as methionine $tRNA^{Met}_{CAU}$, when it was actually aminoacylated by isoleucyl-tRNA synthetases (57). To identify the potential tRNA substrate for *Pf*TilS, we conducted a maximum likelihood phylogenetic analysis (37) encompassing 83 tRNA genes with anticodons for methionine (CAU) and isoleucine (CAU, AAU, UAU, GAU) from archaea, eubacteria, higher eukaryotes, and apicomplexan apicoplast genomes. This analysis revealed a potential shared ancestry between one of the three *P. falciparum* apicoplast tRNA genes harboring a CAU anticodon (PF3D7_API00600) and experimentally validated bacterial TilS tRNA substrate (**Supplementary Figure 5**). Previous studies using footprinting and structural analyses in *E. coli* have identified U33, C34, and A37 in the anticodon loop, the G27+U43 base pair in the anticodon stem, and the C4+G69 and C5+G68 base pairs in the acceptor stem of $tRNA^{Ile}_{CAU}$ as crucial determinants for TilS binding (**Supplementary Figure 6**) (19). Although PF3D7_API00600 tRNA lacks the stem determinants, it possesses the conserved bases within the anticodon loop, making it the best candidate for an apicoplast $tRNA^{Ile}_{CAU}$.

The determinants present in the anticodon and acceptor stems are conserved in γ-proteobacteria but not in other eubacterial tRNAs, including *B. subtilis* (19). This suggests that TilS recognition and discrimination mechanisms between similar tRNAs might vary across organisms. Nonetheless, apicoplast localization of *Pf*TilS and its functional complementation by *Ec*TilS in the apicoplast strongly suggests that at least one of the three apicoplast $tRNA_{CAU}$ isoacceptors is modified by lysidinylation. As demonstrated in bacteria (21), the L modification at the wobble position of $tRNA_{CAU}$ is likely to be sufficient to enable its recognition by isoleucyl-tRNA synthetase rather than methionyl-tRNA synthetase in the apicoplast.

The current study identifies TilS, a tRNA-modifying enzyme localized to the apicoplast in the apicomplexan parasite *P. falciparum*. We demonstrate that TilS activity is required for apicoplast maintenance and parasite survival, presumably due to its crucial role in isoleucine and methionine decoding. These findings establish TilS as a fundamental component of minimal protein translation machinery and inform synthetic biology efforts to design highly reduced

biological systems. These results also provide new insights into apicoplast biology in apicomplexan parasites and unveil a novel vulnerability in several of the important pathogens found in this group of organisms. This vulnerability presents a potential avenue for therapeutic intervention in the fight against malaria, a disease responsible for an estimated 600,000 deaths annually (58). Recent evidence links apicoplast-localized tRNA modifications to response to frontline artemisinin drugs (59), highlighting the potential importance of tRNA modifications in parasite susceptibility to antimalarials. Notably, the identification of ATP-competitive TilS inhibitors in bacteria (60), offers a promising starting point for the discovery of novel antimalarial compounds.

Experimental procedures

Plasmodium falciparum parental parasite line

PfMev^{attB} parental parasites were used for generating knockout and knock-in lines. This parasite line possesses an engineered cytosolic mevalonate pathway for isoprenoid precursor production (29, 38). Additionally, the apicoplast of this parasite line is labeled with a codon-optimized variant of super-folder green fluorescent protein (api-SFG) (42).

Asexual blood stage culture

Asexual-stage *P. falciparum* parasites were aseptically cultured in human O^+ red blood cells (RBC) at a 2% hematocrit using RPMI 1640 medium with L-glutamine (USBiological, MA, USA). The RPMI 1640 medium was supplemented with 12.5 µg/mL hypoxanthine, 20 mM HEPES, 0.2% sodium bicarbonate, 5 g/L Albumax II (Life Technologies, CA, USA), and 25 µg/mL gentamicin. Cultures were maintained at 37°C in 25 cm^2 gassed flasks with a controlled atmosphere of 94% N_2, 3% O_2, and 3% CO_2. Parasitemia was maintained between 2% and 5%. To ensure continuous propagation, cultures were passaged every other day by diluting with fresh medium containing uninfected RBCs.

Construction of transfection plasmids

Codon-modified versions of the *P. falciparum tilS* (*pftilS*) gene, encoding either the full-length or N-terminally truncated protein, were synthesized by Twist Bioscience (CA, USA). Both constructs were flanked by *AvrII* and *PspOMI* restriction enzyme sites and included a C-terminal 3xV5 epitope tag for immunodetection (sequences are available in **Supplementary Figure 7** and **8**). The synthetic *pftilS* genes were cloned into the corresponding restriction sites

within the pCre-FH*-SFG plasmid (61) to generate pCre-*pftilS-3xV5* (full-length *Pf*TilS) and pCre-*trpftilS-3xV5* (N-terminally truncated *Pf*TilS) plasmids.

The *pftilS* gene (PF3D7_0411200) was targeted for deletion using two plasmids: pRSng (29) and pCasG-LacZ (46). To construct the repair plasmid (pRSng-*pftilS*), we amplified two *pftilS* homology arms (HA1, 403 bp; HA2, 569 bp) from *P. falciparum* PfMev^{attB} genomic DNA using specific primers (**Supplementary Table 1**). HA1 and HA2 were inserted into the *NotI* and *NgoMIV* restriction sites, respectively, of pRSng by In-Fusion (Clontech Laboratories, CA, USA) ligation independent cloning (LIC). The guide RNA (gRNA) sequence targeting *pftilS* (20 bp) was synthesized as 5'-phosphorylated oligonucleotides, annealed, and inserted into the *BsaI* sites of pCasG-LacZ using ligase dependent cloning to generate the pCasG-*pftilS*gRNA plasmid.

For generation of the *ectilS* knock-in plasmid, we amplified the *ectilS* gene (NCBI gene ID 944889) from *E. coli* genomic DNA with the following primer pair: EcTilS.InF.F and EcTilS.InF.R (**Supplementary Table 1**). The *ectilS* amplicon was inserted by LIC in place of the *bsmnmA* gene in plasmid pCLD-*bsmnmA-mcherry-10xapt* (43) to yield the pCLD-*ectilS-mcherry-10xapt* plasmid. All restriction enzymes were sourced from New England Biolabs Inc, MA, USA. Sanger sequencing was performed on all constructs to verify sequence fidelity.

Parasite transfections

To generate the Δ*pftilS* transgenic line, we transfected PfMev^{attB} parasites with the pRSng-*pftilS* and pCasG-*pftilS*gRNA plasmids (75 µg each) using an established transfection protocol (39). Briefly, 400 µL of RBCs were electroporated with the plasmid mixture by low-voltage electroporation. The transfected RBCs were then mixed with 1.5 mL of PfMev^{attB} parasites (mostly mid-trophozoite to early schizont stage) and cultured in complete medium with 50 µM mevalonate (Racemic mevalonolactone; Catalog #M4667, Sigma-Aldrich, MO, USA) for 48 h. To select for parasites that underwent successful homologous recombination events at the *pftilS* locus, the culture medium was subsequently supplemented with 1.5 µM DSM1 (BEI Resources, VA, USA), 2.5 nM WR99210 (Jacobus Pharmaceuticals, NJ, USA), and 50 µM mevalonate for a period of seven days. After this selection period, cultures were maintained in complete medium with 50 µM mevalonate until parasite emergence. Once the parasites appeared, the cultures were maintained in complete medium with 2.5 nM WR99210 and 50 µM mevalonate.

We co-transfected RBCs with pCre-*pftilS-3xV5*, pCre-*trpftilS-3xV5* or pCLD-*ectilS-mCherry-10xapt* plasmids, respectively, with the pINT plasmid (62) encoding the mycobacteriophage integrase. The integrase facilitates recombination of the attP site found in the expression constructs with the attB site in the parasite genome. The transfected RBCs were then infected with PfMev^{attB} parasites (38) and cultured with 1.25 µg/mL blasticidin (Corning Inc, NY, USA) and 0.50 µM anhydrous tetracycline (aTc, Cayman Chemical, MI, USA) for seven days to select for parasites with successful integration events. After seven days, cultures were maintained in complete medium with aTc until parasite emergence. Once parasites reappeared, the cultures were maintained with 1.25 µg/mL blasticidin and 0.50 µM aTc.

For *ectilS*$^{+}$Δ*pftilS* transgenic parasite generation, we used the same Cas9 and pRSng repair plasmids used for the Δ*pftilS* line. Growth medium supplemented with 1.5 µM DSM1, 2.5 nM WR99210, 1.25 µg/mL blasticidin, and 0.50 µM aTc was used for the initial seven days of selection, after which the cultures were switched to growth medium containing blasticidin and aTc. Upon parasite appearance, all cultures were maintained in medium containing WR99210, blasticidin, and aTc.

Genotype confirmation

Parasite lysates were prepared from parental or transgenic lines by incubation at 90 °C for 5 min. These lysates served as templates for all subsequent genotype confirmation PCRs. For confirmation of Δ*pftilS* and *ectilS*$^{+}$Δ*pftilS* genotypes, we used specific primer pairs (primer sequences are available in **Supplementary Table 1**) to amplify both the 5'- and 3'- ends (designated Δ5' and Δ3', respectively) of the disrupted *pftilS* locus and the corresponding regions (designated 5' and 3', respectively) of the native locus. The expected amplicon sizes for each primer pair are provided in **Figure 3A**.

For *pftilS*$^{+}$, *trpftilS*$^{+}$ or *ectilS*$^{+}$ genotype confirmations, specific primers (sequences available in **Supplementary Table 1**) were used to amplify the attL and attR recombination junctions flanking the integrated plasmids. Additionally, we amplified the unaltered attB site in the parental parasite genome as a control. The anticipated sizes of the PCR products are indicated in **Figures 2B and 4A**.

Confirmation of apicoplast genome loss

We used the apicoplast-encoded *sufB* gene (PF3D7_API04700) as a proxy for detecting the apicoplast genome. The gene was amplified by PCR with a specific primer pair listed in

Supplementary Table 1. As controls, genes from the nuclear genome (*ldh*, PF3D7_1324900) and the mitochondrial genome (*cox1*, PF3D7_MIT02100) were amplified with corresponding primer pairs (sequences available in **Supplementary Table 1**). Parasite lysates of the parental line were used as positive controls for apicoplast genome detection. The expected amplicon sizes for *ldh*, *sufB*, and *cox1* are 520 bp, 581 bp, and 761 bp, respectively.

Immunoblot

Asynchronous parental and *ectilS*$^{+}$ parasite cultures were washed three times with cold complete medium. We then treated the washed cultures with 0.15% (w/v) saponin in cold phosphate-buffered saline (PBS, pH 7.4) for 10 minutes on ice. This step permeabilizes the RBC and parasitophorous vacuolar membranes, allowing access to the intracellular parasites (63). Following saponin treatment, intact parasites were pelleted by centrifugation at 1,940 x g for 10 min at 4 °C. The parasite pellets were washed three additional times with cold PBS. The isolated parasites were then either used immediately or snap-frozen in liquid nitrogen and stored at -80 °C for later use.

Saponin-isolated parasites were resuspended in 1x NuPAGE LDS sample buffer (Thermo Fisher Scientific, MA, USA) containing 2% β-mercaptoethanol and boiled for 5□min to ensure complete protein denaturation and solubilization. The lysed parental and *ectilS*$^{+}$ parasite samples were resolved by sodium dodecyl sulfate-polyacrylamide gel electrophoresis (SDS-PAGE) using 4-12% gradient reducing gels. Following SDS-PAGE, the separated proteins were transferred electrophoretically to nitrocellulose membranes. The membranes were blocked with 5% non-fat dry milk in PBS containing 0.1% Tween-20 (Milk/PBST) for 1 h at room temperature to minimize non-specific antibody binding. Following blocking, the membranes were incubated overnight at 4 °C with primary rabbit anti-mCherry antisera (38) (diluted 1:5000 in Milk/PBST) to detect *Ec*TilS-mCherry fusion protein (expected molecular weight 91 kDa). The membranes were then washed and incubated with donkey anti-rabbit horseradish peroxidase (HRP)-conjugated secondary antibodies (diluted 1:10000 in Milk/PBST; Catalog # 31458, ThermoFisher Scientific, MA, USA) for 1 h at room temperature. Chemiluminescent signal was developed with SuperSignal West Pico chemiluminescent substrate (Catalog # 34577, ThermoFisher Scientific, MA, USA) according to the manufacturer's instructions and detected on autoradiography film.

To ensure equal protein loading across samples, the membranes were stripped of antibodies using a 5 min incubation with 200 mM glycine buffer (pH 2.0) at room temperature. The stripped membranes were then re-blocked with 5% Milk/PBST and probed with primary anti-Aldolase mouse monoclonal antibody (diluted 1:25000; a gift from David J. Sullivan, Johns Hopkins Bloomberg School of Public Health) followed by sheep anti-mouse HRP-conjugated secondary antibody (diluted 1:10000; Catalog # GENA931, Millipore Sigma, MO, USA). The chemiluminescent detection steps were repeated as described above.

Immunofluorescence assays and live cell microscopy

For immunofluorescence assays, we fixed and permeabilized *pftilS*$^{+}$ and *trpftilS*$^{+}$ parasites as described previously (64) with minor modifications. Briefly, infected RBCs from 250 µL of culture (~5% parasitemia in 2% hematocrit) were harvested by centrifugation and resuspended in 300 µL of 4% electron microscopy (EM) grade paraformaldehyde and 0.0075% EM grade glutaraldehyde in PBS (pH 7.4) for fixation. The fixation step was carried out for 30 min at 37 °C while shaking at 225 rpm. Following fixation, the cells were permeabilized using 0.1% Triton X-100 in PBS for 10 minutes on a 3D-rocker. After a 2 h blocking step with 3% bovine serum albumin (BSA) in PBS at room temperature on a 3D-rocker to prevent non-specific binding, cells were incubated overnight at 4 °C with 1:500 rabbit anti-ACP antibody (65) and 1:1000 mouse anti-V5 (SV5-Pk1) antibody (Catalogue # ab27671, Abcam, MA, USA) on an orbital shaker. After the overnight incubation, the cells were washed with PBS three times and then incubated for 2 h with 1:1500 goat anti-rabbit Alexa 488 (Catalogue # A-11034, ThermoFisher Scientific, MA, USA) and 1:1500 goat anti-mouse Alexa 594 (Catalogue # A-11032, ThermoFisher Scientific, MA, USA) secondary antibodies in PBS with 3% BSA on a 3D-rocker. After three washes with PBS, the cells were mounted on coverslips with ProLong Gold 4′, 6-diamidino-2-phenylindole (DAPI) antifade reagent (Catalogue # P36935, ThermoFisher Scientific, MA, USA) and sealed with nail polish.

For live cell imaging of the Δ*pftilS* transgenic line, we incubated 100 µL of asynchronous parasites of ~5% parasitemia and 2% hematocrit with 1 µg/mL DAPI (Invitrogen, CA, USA) and 30 nM MitoTracker Red CMX-Ros (Invitrogen, CA, USA) for 30 min at 37 °C. Following incubation, the cells were washed three times with complete medium, with a 5 min incubation at 37 °C after each wash step. After the final wash, the parasites were resuspended in 20 µL of complete medium, placed on a slide, and sealed under a coverslip using wax. For live cell

imaging of the *ectilS*$^{+}$ and *ectilS*$^{+}$Δ*pftilS* parasite lines, cells were stained with 1 µg/mL DAPI only.

All images were captured using a Zeiss AxioImager M2 microscope (Carl Zeiss Microscopy, LLC, NY, USA) equipped with a Hamamatsu ORCA-R2 camera (Hamamatsu Photonics, Hamamatsu, Japan) and a 100x/1.4 NA objective lens. A series of images were obtained spanning 5 µm along the z-axis with a spacing of 0.2 µm between each image. Subsequently, an iterative restoration algorithm implemented within Volocity software (PerkinElmer, MA, USA) was used to deconvolve the images to report a single image in the z-plane.

Parasite growth assay

Parasite growth was monitored using an Attune Nxt Flow Cytometer (Thermo Fisher Scientific, MA, USA) as previously described (29, 66). For determining the growth dependence on mevalonate presented in **Figure 3E**, we cultured Δ*pftilS* parasites in the presence or absence of 50 µM mevalonate, and in the experiment presented in **Figure 5C**, cultures were grown in the presence or absence of 50 µM mevalonate with 0.5 µM aTc supplementation in both conditions. In both experiments, the cultures were seeded at 0.5% initial parasitemia and 2% hematocrit in a total volume of 250 µL, in quadruplicate for each condition. Parasite growth was monitored every 24 h over four days following SYBR green I (Catalogue # S7563, ThermoFisher Scientific, MA, USA) staining. For growth assays presented in **Figures 5F**, we grew the *ectilS*$^{+}$Δ*pftilS* parasites in the presence of 0.5 µM aTc and absence of *Shield1* (Catalogue # AOB1848, Aobious Inc, MA, USA) (permissive condition) or in the absence of aTc and presence of 0.5 µM *Shield1* (nonpermissive condition). In this experiment, parasite growth was monitored over eight days. On day four, the cultures were diluted 1:10. Data from two independent biological replicates (each in quadruplicate) of the indicated parasite lines were analyzed using a two-way ANOVA with a Sidak-Bonferroni correction in Prism V8.4 (GraphPad Software, CA, USA).

The growth of the *ectilS*$^{+}$ (**Figure 4E**) and *ectilS*$^{+}$Δ*pftilS* (**Figure 5F**) lines were compared to that of the parental PfMev^{attB} parasite line. Asynchronous parasite cultures were seeded in duplicate at a standardized initial parasitemia of 0.5% and a hematocrit of 2% in 96-well plates with a total volume of 200 µL per well. In all cases the media was supplemented with 0.5 µM aTc. Following a 48-h incubation (corresponding to a complete growth cycle), final parasitemia was determined using flow cytometry as described above. The growth rate was

calculated by dividing the final parasitemia by the initial parasitemia, resulting in a fold-change value per growth cycle. This experiment was repeated for at least five growth cycles for each parasite line and the data are presented as median fold increase per growth cycle.

Bioinformatics

Multiple sequence alignment (MSA) of TilS orthologs was performed using the ClustalW program implemented in MEGA11 software (67). The MSA included the following full-length protein sequences: *P. falciparum* (*Pf* TilS, PlasmoDB ID: PF3D7_0411200), *Synechocystis* sp. (*Sy* TilS, Uniprot ID: P74192), *Aquifex aeolicus* (*Aa* TilS, Uniprot ID: O67728), *Mycoplasma genitalium* (*Mg* TilS, Uniprot ID: P47330), *E. coli* (*Ec* TilS, Uniprot ID: P52097), *Geobacillus kaustophilus* (*Gk* TilS, Uniprot ID: Q5L3T3), and *Arabidopsis thaliana* (*At* RSY3, Uniprot ID: F4J7P7). MSA output was visualized using Boxshade (https://junli.netlify.app/apps/boxshade/) to highlight conserved residues.

Phylogenetic analyses presented in **Supplementary Figures 3 and 5** were performed using MEGA11 software (67). We used the maximum likelihood method incorporating the JTT matrix-based model (37). To assess the robustness of the inferred tree topology, 1000 bootstrap replicates were performed. The resulting tree with the highest likelihood score is presented. The proteins used for phylogenetic analysis presented in **Supplementary Figure 3** are listed in **Supplementary Table 2**, and the tRNAs used for analysis presented in **Supplementary Figure 5** are listed in **Supplementary Table 3**.

The secondary structures of tRNAs presented in **Supplementary Figure 6** were generated using tRNAscan-SE online program (68).

Acknowledgments

We are grateful to David J. Sullivan (Johns Hopkins Bloomberg School of Public Health) for his generous gift of the mouse anti-aldolase monoclonal antibody. We extend our sincere appreciation to the students enrolled in Biology of Parasitism 2021 for their contributions to this study. Financial support for this research was provided by the National Institutes of Health grant R01 AI125534 (S.T.P.), the Johns Hopkins Malaria Research Institute postdoctoral fellowship (R.E.), Samuel Jordan Graham postdoctoral fellowship (R.E.), the Johns Hopkins Malaria Research Institute, and Bloomberg Philanthropies. The funding agencies did not exert any influence on the design of the study, the collection or analysis of data, the decision to publish the findings, or the preparation of the manuscript.

Author contributions

R.E. and S.T.P. designed and performed research, analyzed data, and wrote the manuscript.

References

1. J. M. Ogle, F. V. Murphy, M. J. Tarry, V. Ramakrishnan, Selection of tRNA by the ribosome requires a transition from an open to a closed form. *Cell* **111**, 721-732 (2002).
2. C. A. Hutchison, 3rd *et al.*, Design and synthesis of a minimal bacterial genome. *Science* **351**, aad6253 (2016).
3. G. M. Bennett, N. A. Moran, Small, smaller, smallest: the origins and evolution of ancient dual symbioses in a Phloem-feeding insect. *Genome Biol Evol* **5**, 1675-1688 (2013).
4. N. Arisue *et al.*, The *Plasmodium* apicoplast genome: conserved structure and close relationship of *P. ovale* to rodent malaria parasites. *Mol Biol Evol* **29**, 2095-2099 (2012).
5. C. Aurrecoechea *et al.*, PlasmoDB: a functional genomic database for malaria parasites. *Nucleic Acids Res* **37**, D539-D543 (2008).
6. R. Elahi, S. T. Prigge, New insights into apicoplast metabolism in blood-stage malaria parasites. *Curr Opin Microbiol* **71**, 102255 (2023).
7. P. Preiser, D. H. Williamson, R. J. Wilson, tRNA genes transcribed from the plastid-like DNA of *Plasmodium falciparum*. *Nucleic Acids Res* **23**, 4329-4336 (1995).
8. S. Alkatib *et al.*, The contributions of wobbling and superwobbling to the reading of the genetic code. *PLoS Genet* **8**, e1003076 (2012).
9. G. R. Björk, "Biosynthesis and function of modified nucleosides" in tRNA. (1994), https://doi.org/10.1128/9781555818333.ch11, pp. 165-205.
10. H. Grosjean *et al.*, Predicting the minimal translation apparatus: lessons from the reductive evolution of mollicutes. *PLoS Genet* **10**, e1004363 (2014).
11. V. de Crécy-Lagard, C. Marck, H. Grosjean, Decoding in *Candidatus Riesia pediculicola*, close to a minimal tRNA modification set? *Trends Cell Mol Biol* **7**, 11-34 (2012).
12. P. Boccaletto *et al.*, MODOMICS: a database of RNA modification pathways. *Nucleic Acids Res* **46**, D303-D307 (2018).
13. M. Kuratani *et al.*, Structural basis of the initial binding of $tRNA^{Ile}$ lysidine synthetase TilS with ATP and L-lysine. *Structure* **15**, 1642-1653 (2007).
14. K. Nakanishi *et al.*, Structural basis for translational fidelity ensured by transfer RNA lysidine synthetase. *Nature* **461**, 1144-1148 (2009).
15. K. Nakanishi *et al.*, Structural basis for lysidine formation by ATP pyrophosphatase accompanied by a lysine-specific loop and a tRNA-recognition domain. *Proc Natl Acad Sci USA* **102**, 7487–7492 (2005).
16. T. Numata, Mechanisms of the tRNA wobble cytidine modification essential for AUA codon decoding in prokaryotes. *Biosci Biotechnol Biochem* **79**, 347-353 (2015).
17. A. Soma *et al.*, An RNA-modifying enzyme that governs both the codon and amino acid specificities of isoleucine tRNA. *Mol Cell* **12**, 689-698 (2003).
18. T. Suzuki, K. Miyauchi, Discovery and characterization of $tRNA^{Ile}$ lysidine synthetase (TilS). *FEBS Lett* **584**, 272-277 (2010).

19. Y. Ikeuchi *et al.*, Molecular mechanism of lysidine synthesis that determines tRNA identity and codon recognition. *Mol Cell* **19**, 235-246 (2005).
20. J. Moriya *et al.*, A novel modified nucleoside found at the first position of the anticodon of methionine tRNA from bovine liver mitochondria. *Biochemistry* **33**, 2234-2239 (1994).
21. T. Muramatsu *et al.*, Codon and amino-acid specificities of a transfer RNA are both converted by a single post-transcriptional modification. *Nature* **336**, 179-181 (1988).
22. T. Muramatsu *et al.*, A novel lysine-substituted nucleoside in the first position of the anticodon of minor isoleucine tRNA from *Escherichia coli*. *J Biol Chem* **263**, 9261-9267 (1988).
23. J. Matsugi, K. Murao, H. Ishikura, Characterization of a *B. subtilis* minor isoleucine tRNA deduced from tDNA having a methionine anticodon CAT. *J Biochem* **119**, 811-816 (1996).
24. R. Gil, J. Peretó, Small genomes and the difficulty to define minimal translation and metabolic machineries. *Front Ecol Evol* **3** (2015).
25. R. Gil, F. J. Silva, J. Peretó, A. Moya, Determination of the core of a minimal bacterial gene set. *Microbiol Mol Biol Rev* **68**, 518-537 (2004).
26. M. J. Garzón, M. Reyes-Prieto, R. Gil, The minimal translation machinery: what we can learn from naturally and experimentally reduced genomes. *Front Microbiol* **13** (2022).
27. A. C. Forster, G. M. Church, Towards synthesis of a minimal cell. *Mol Syst Biol* **2**, 45 (2006).
28. R. F. Waller, M. B. Reed, A. F. Cowman, G. I. McFadden, Protein trafficking to the plastid of *Plasmodium falciparum* is via the secretory pathway. *EMBO J* **19**, 1794-1802 (2000).
29. R. P. Swift *et al.*, A mevalonate bypass system facilitates elucidation of plastid biology in malaria parasites. *PLoS Pathog* **16**, e1008316 (2020).
30. C. S. Ng *et al.*, tRNA epitranscriptomics and biased codon are linked to proteome expression in *Plasmodium falciparum*. *Mol Syst Biol* **14**, e8009 (2018).
31. N. M. Fast, J. C. Kissinger, D. S. Roos, P. J. Keeling, Nuclear-encoded, plastid-targeted genes suggest a single common origin for apicomplexan and dinoflagellate plastids. *Mol Biol Evol* **18**, 418-426 (2001).
32. J. Janouskovec, A. Horák, M. Oborník, J. Lukes, P. J. Keeling, A common red algal origin of the apicomplexan, dinoflagellate, and heterokont plastids. *Proc Natl Acad Sci USA* **107**, 10949-10954 (2010).
33. R. B. Moore *et al.*, A photosynthetic alveolate closely related to apicomplexan parasites. *Nature* **451**, 959-963 (2008).
34. B. J. Foth *et al.*, Dissecting apicoplast targeting in the malaria parasite *Plasmodium falciparum*. *Science* **299**, 705-708 (2003).
35. J. Jumper *et al.*, Highly accurate protein structure prediction with AlphaFold. *Nature* **596**, 583-589 (2021).
36. M. Varadi *et al.*, AlphaFold Protein Structure Database: massively expanding the structural coverage of protein-sequence space with high-accuracy models. *Nucleic Acids Res* **50**, D439-D444 (2021).
37. D. T. Jones, W. R. Taylor, J. M. Thornton, The rapid generation of mutation data matrices from protein sequences. *Comput Appl Biosci* **8**, 275-282 (1992).
38. R. P. Swift, K. Rajaram, H. B. Liu, S. T. Prigge, Dephospho-CoA kinase, a nuclear-encoded apicoplast protein, remains active and essential after *Plasmodium falciparum* apicoplast disruption. *EMBO J* **40**, e107247 (2021).
39. M. D. Spalding, M. Allary, J. R. Gallagher, S. T. Prigge, Validation of a modified method for Bxb1 mycobacteriophage integrase-mediated recombination in *Plasmodium falciparum* by localization of the H-protein of the glycine cleavage complex to the mitochondrion. *Mol Biochem Parasitol* **172**, 156-160 (2010).

40. M. J. Boucher *et al.*, Integrative proteomics and bioinformatic prediction enable a high-confidence apicoplast proteome in malaria parasites. *PLoS Biol* **16**, e2005895 (2018).
41. M. Ghorbal *et al.*, Genome editing in the human malaria parasite *Plasmodium falciparum* using the CRISPR-Cas9 system. *Nat Biotechnol* **32**, 819-821 (2014).
42. A. D. Roberts, S. C. Nair, A. J. Guerra, S. T. Prigge, Development of a conditional localization approach to control apicoplast protein trafficking in malaria parasites. *Traffic* **20**, 571-582 (2019).
43. R. P. Swift, R. Elahi, K. Rajaram, H. B. Liu, S. T. Prigge, The *Plasmodium falciparum* apicoplast cysteine desulfurase provides sulfur for both iron-sulfur cluster assembly and tRNA modification. *Elife* **12**, e84491 (2023).
44. E. Yeh, J. L. DeRisi, Chemical rescue of malaria parasites lacking an apicoplast defines organelle function in blood-stage *Plasmodium falciparum*. *PLoS Biol.* **9**, e1001138 (2011).
45. S. M. Ganesan, A. Falla, S. J. Goldfless, A. S. Nasamu, J. C. Niles, Synthetic RNA–protein modules integrated with native translation mechanisms to control gene expression in malaria parasites. *Nat Commun* **7**, 10727 (2016).
46. K. Rajaram, H. B. Liu, S. T. Prigge, Redesigned TetR-Aptamer system to control gene expression in *Plasmodium falciparum*. *mSphere* **5** (2020).
47. R. P. Swift *et al.*, The NTP generating activity of pyruvate kinase II is critical for apicoplast maintenance in *Plasmodium falciparum*. *Elife* **9** (2020).
48. A. P. de Koning, P. J. Keeling, The complete plastid genome sequence of the parasitic green alga *Helicosporidium* sp. is highly reduced and structured. *BMC Biol* **4**, 12 (2006).
49. M. Fages-Lartaud, M. F. Hohmann-Marriott, Overview of tRNA modifications in chloroplasts. *Microorganisms* **10** (2022).
50. The Arabidopsis Genome Initiative, Analysis of the genome sequence of the flowering plant *Arabidopsis thaliana*. *Nature* **408**, 796-815 (2000).
51. K. Gołębiewska, P. Gregorová, L. P. Sarin, P. Gawroński, Deciphering the RNA modification landscape in *Arabidopsis* chloroplast tRNAs and rRNAs reveals a blend of ancestral and acquired characteristics. *bioRxiv* 10.1101/2024.06.14.598963, 2024.2006.2014.598963 (2024).
52. A. J. Reid *et al.*, Genomic analysis of the causative agents of coccidiosis in domestic chickens. *Genome Res.* **24**, 1676-1685 (2014).
53. O. S. Harb, D. S. Roos, "ToxoDB: Functional genomics resource for *Toxoplasma* and related organisms" in *Toxoplasma gondii*: Methods and Protocols, C. J. Tonkin, Ed. (Springer US, New York, NY, 2020), 10.1007/978-1-4939-9857-9_2, pp. 27-47.
54. L. Berná *et al.*, Reevaluation of the *Toxoplasma gondii* and *Neospora caninum* genomes reveals misassembly, karyotype differences, and chromosomal rearrangements. *Genome Res* **31**, 823-833 (2021).
55. A. Garg *et al.*, Sequence and annotation of the apicoplast genome of the human pathogen *Babesia microti*. *PLoS One* **9**, e107939 (2014).
56. M. J. Gardner *et al.*, Genome sequence of *Theileria parva*, a bovine pathogen that transforms lymphocytes. *Science* **309**, 134-137 (2005).
57. C. Köhrer *et al.*, Identification and characterization of a tRNA decoding the rare AUA codon in *Haloarcula marismortui*. *RNA* **14**, 117-126 (2008).
58. World Health Organization (2023) World Malaria Report 2023. (World Health Organization, Geneva).
59. J. L. Small-Saunders *et al.*, tRNA modification reprogramming contributes to artemisinin resistance in *Plasmodium falciparum*. *Nat Microbiol* **9**, 1483-1498 (2024).
60. A. B. Shapiro *et al.*, Discovery of ATP-competitive inhibitors of $tRNA^{Ile}$ lysidine synthetase (TilS) by high-throughput screening. *J Biomol Screen* **19**, 1137-1146 (2014).

61. K. Rajaram, S. G. Tewari, A. Wallqvist, S. T. Prigge, Metabolic changes accompanying the loss of fumarate hydratase and malate-quinone oxidoreductase in the asexual blood stage of *Plasmodium falciparum*. *J Biol Chem* **298**, 101897 (2022).
62. L. J. Nkrumah *et al.*, Efficient site-specific integration in *Plasmodium falciparum* chromosomes mediated by mycobacteriophage Bxb1 integrase. *Nat Methods* **3**, 615-621 (2006).
63. S. R. Christophers, J. D. Fulton, Experiments with isolated malaria parasites (*Plasmodium knowlesi*) free from red cells. *Ann Trop Med Parasitol* **33**, 161-170 (1939).
64. J. R. Gallagher, K. A. Matthews, S. T. Prigge, *Plasmodium falciparum* apicoplast transit peptides are unstructured in vitro and during apicoplast import. *Traffic* **12**, 1124-1138 (2011).
65. J. R. Gallagher, S. T. Prigge, *Plasmodium falciparum* acyl carrier protein crystal structures in disulfide-linked and reduced states and their prevalence during blood stage growth. *Proteins* **78**, 575-588 (2010).
66. S. G. Tewari *et al.*, Metabolic adjustments of blood-stage *Plasmodium falciparum* in response to sublethal pyrazoleamide exposure. *Sci Rep* **12**, 1167 (2022).
67. K. Tamura, G. Stecher, S. Kumar, MEGA11: Molecular Evolutionary Genetics Analysis Version 11. *Mol Biol Evol* **38**, 3022-3027 (2021).
68. T. M. Lowe, P. P. Chan, tRNAscan-SE On-line: Integrating search and context for analysis of transfer RNA genes. *Nucleic Acids Res* **44**, W54-W57 (2016).

Figure legends

Figure 1. *Plasmodium falciparum* contains a putative tRNA-isoleucine lysidine synthetase (TilS)

(A) Chemical structure of lysidine (L). (B) The $tRNA_{CAU}$ binds the AUG codon and is charged with Methionine (Met), unless tRNA-isoleucine lysidine synthetase (TilS) modifies C34 to L34 using L-lysine (L-Lys) and ATP as substrates. The $tRNA_{CAU}$ with the LAU anticodon recognizes AUA codons, and is charged with isoleucine (Ile). (C) Two tRNAs in the apicoplast genome decode Met and Ile codons. $tRNA_{CAU}$ can potentially decode both AUA and AUG codons (highlighted in yellow). (D) Met and Ile codon usage in *Plasmodium* apicoplast-genome coded proteins. Yellow highlight shows the most frequently used Ile codon. (E) Residues important for tRNA binding (red symbols) and lysine binding (black symbols) are mapped on *Escherichia coli* TilS (432 residues) and a putative 1245 residue *P. falciparum* TilS. TP, apicoplast targeting peptide. (F) AlphaFold predicted structure of *Pf* TilS residues 181-1245 (right) shows a folding pattern similar to *E. coli* TilS structure 1NI5 (left).

Figure 2. *Plasmodium falciparum* TilS localizes to the apicoplast

(A) Scheme showing synthetic *Pf*TilS constructs. The scale at the top shows the length (in amino acid residues, aa) of expected protein for full-length or N-terminally truncated *Pf*TilS. (B) Schematic illustration (not to scale) of pCre plasmid insertion into the attB locus of $PfMev^{attB}$ parasites to generate *pftilS*$^{+}$ or *trpftilS*$^{+}$ parasites. A bidirectional promoter drives the expression of blasticidin-*S*-deaminase (*bsd*) and the *Pf*TilS construct (*pftils-3xV5* or *trpftilS-3xV5*). Plasmid pINT expresses integrase (*int*) for catalyzing attB/attP recombination. Primer pairs (black half arrow) for PCR amplification of the attB region of the parental line and the recombinant attL and attR regions with expected amplicon sizes are depicted. Refer to **Supplementary Table 1** for primer sequences. (C). PCR amplification of attL and attR regions confirms plasmid integration in both *pftilS*$^{+}$ and *trpftilS*$^{+}$ parasites. Amplification of the attB region from the $PfMev^{attB}$ parasite line (parental) was used as a control. Expected amplicon size with corresponding primer pairs are depicted in (B). DNA markers are in kilobases (kb). (D) Immunofluorescence microscopy demonstrates colocalization of full-length *Pf*TilS (*pftilS*$^{+}$) tagged with a C-terminal 3xV5 epitope (magenta) with the apicoplast marker ACP (acyl carrier protein, green). Truncated *Pf*TilS (*trpftilS*$^{+}$) exhibits a diffuse cytosolic distribution (magenta) in

the bottom panels. DAPI staining (blue) marks nuclear DNA in both panels. Images represent a field of 10 μm x 10 μm.

Figure 3. *Pf*TilS is essential for apicoplast maintenance and parasite survival

(A) Schematic illustrating double-crossover homologous recombination for *pftilS* gene knockout. A repair plasmid (pRSng-*pftilS*) harboring two homology arms (HAs) flanks the desired modification site within the native *pftilS* locus. Cas9 endonuclease with guide RNA (Cas9-*pftilS*gRNA plasmid) introduces a double-stranded break (blue arrow) in the native locus, facilitating homologous recombination with the repair plasmid leading to the recombinant Δ*pftilS* locus. Primer positions and directions (black half arrows) for confirming gene knockout are indicated. Refer to **Supplementary Table 1** for primer sequences. *hdhfr*, human dihydrofolate reductase; *ydhod*, yeast dihydroorotate dehydrogenase. (B) Genotyping PCR verifies *pftilS* deletion in Δ*pftilS* parasites, shown by the presence of amplicons for the Δ5' and Δ3' loci at the integration site, but not for the native loci (5' and 3') found in the PfMev^{attB} (parental) parasites. The primers and expected amplicon sizes are depicted in (A). (C) Attempted PCR amplification of *ldh*, *sufB*, and *cox1* genes of the parasite nuclear (N), apicoplast (A), and mitochondrial (M) genomes, respectively, in Δ*pftilS* and PfMev^{attB} (parental) parasites. Lack of an amplicon for *sufB* in the Δ*pftilS* parasites indicates the loss of the apicoplast genome. Refer to **Supplementary Table 1** for primer names and sequences and materials and methods for expected amplicon sizes. (D) Representative epifluorescence microscopy images of Δ*pftilS* parasites shows multiple discrete vesicles (top panel) demonstrating a disrupted apicoplast, compared to an intact apicoplast in PfMev^{attB} parasites (parental, bottom panel). Api-SFG protein (green) marks the apicoplast, the mitochondrion is stained with MitoTracker (red), and nuclear DNA is stained with DAPI (blue). Each image depicts a field of 10 μm ×10 μm. (E) The Δ*pftilS* parasites are dependent on mevalonate (Mev) for growth. Asynchronous parasites were grown with or without 50 μM Mev and parasitemia was monitored every 24 h by flow cytometry for 4 days. Data points represent daily mean parasitemia ± standard error of mean (SEM) from two independent biological replicates, each with four technical replicates. In (B) and (C), DNA markers are in kilobases (kb).

Figure 4. *Escherichia coli* TilS can be expressed in the *P. falciparum* apicoplast

(A) Schematic illustration of pCLD-*ectilS*-mCherry-10xapt plasmid insertion into the attB locus of PfMev^{attB} parasites to generate the *ectilS*$^{+}$ line. The *tetR-dozi* inducible system regulator and blasticidin-*S*-deaminase (*bsd*) are separated by a T2A viral skip peptide (not shown). The *cld-ectilS-mcherry-10xapt* and *tetR-dozi-2A-bsd* cassettes are expressed under a single bidirectional promoter. This plasmid was co-transfected with the pINT plasmid, which expresses integrase (*int*) for catalyzing attB/attP recombination. Primer pairs (black half arrows) for PCR amplification of the attB region of the parental line and the recombinant attL and attR regions are marked along with the expected amplicon sizes. Refer to **Supplementary Table 1** for primer sequences. cld, conditional localization domain. (B) Expected transcript and protein in *ectilS*$^{+}$. (C) PCR amplification of attL and attR regions confirms plasmid integration in *ectilS*$^{+}$ parasites. Amplification of the attB region from the PfMev^{attB} parasite line (parental) was used as a control. Expected amplicon size with corresponding primer pairs are depicted in (A). DNA markers are in kilobases (kb). (D) Immunoblot of saponin-isolated PfMev^{attB} (parental) and *ectilS*$^{+}$ parasite lysates with anti-mCherry antibody (top panel) confirms expression of *Ec*TilS-mCherry fusion protein (expected molecular weight 91 kDa, black arrowhead). Anti-aldolase immunoblot shows relative loading levels (bottom panel). Protein markers are in kilodaltons (kDa). Refer to **Supplementary Figure 4** for the uncropped blot image. (E) Growth comparison of *ectilS*$^{+}$ and the PfMev^{attB} parental line with 0.5 µM aTc supplementation shows no significant growth difference (two-way ANOVA, Mann-Whitney U test). Asynchronous parasites were cultured for a complete growth cycle (~48 h), after which parasitemia was determined. The ratio of the final and initial parasitemia (fold increase) represents the growth rate. Data are from five biological replicates, each with technical duplicates; *bars*, median fold increase. (F) Representative epifluorescence microscopy images of *ectilS*$^{+}$ parasites confirm the colocalization of *Ec*TilS-mCherry fusion protein (magenta) with the apicoplast api-SFG marker (green). The nuclear DNA is stained with DAPI (blue). Each image depicts a field of 10 µm ×10 µm.

Figure 5. *Escherichia coli* TilS complements the loss of *P. falciparum* TilS

(A) The anticipated outcome of *pftilS* deletion in the *ectilS*$^{+}$ parasite line is depicted in the schematic. *E. coli* TilS complementation of parasite TilS lysidinylation activity is sufficient for proper apicoplast protein translation and maintenance. (B) Genotyping PCR verifies *pftilS*

deletion in *ectilS*$^{+}$Δ*pftilS* parasites, shown by the presence of amplicons for the Δ5' and Δ3' loci at the integration site, but not for the native loci (5' and 3') found in the *ectilS*$^{+}$ (parental) parasites. The primers and expected amplicon sizes are depicted in **Figure 3A**. (C) Growth of *ectilS*$^{+}$Δ*pftilS* parasites does not require mevalonate (Mev). Asynchronous parasites were grown with or without 50 μM Mev in media containing 0.5 μM aTc. Parasitemia was monitored every 24 h by flow cytometry for 4 days. Data points represent daily mean parasitemia ± SEM from two independent biological replicates, each with four technical replicates; n.s., non-significant, two-way ANOVA (Sidak-Bonferroni method), $p>0.05$. (D) Representative epifluorescence microscopy images of *ectilS*$^{+}$Δ*pftilS* parasites shows an intact apicoplast. (E) PCR detection of *ldh*, *sufB*, and *cox1* genes of the parasite nuclear (N), apicoplast (A), and mitochondrial (M) genomes, respectively, in *ectilS*$^{+}$Δ*pftilS* and *ectilS*$^{+}$ (parental) parasites. Successful amplification of *sufB* in *ectilS*$^{+}$Δ*tilS* parasites indicates the presence of the apicoplast genome. (F) Growth comparison of *ectilS*$^{+}$Δ*pftilS* and the PfMev^{attB} parental line with 0.5 μM aTc supplementation shows no significant growth difference (two-way ANOVA, Mann-Whitney U test). Asynchronous parasites were cultured for a complete growth cycle (~48 h), after which parasitemia was determined. The ratio of the final and initial parasitemia (fold increase) represents the growth rate. Data are from five biological replicates, each with technical duplicates; *bars*, median fold increase. (G) Schematic depicts the inducible control of an *Ec*TilS-mCherry fusion protein within the apicoplast of *ectilS*$^{+}$Δ*pftilS* parasites. The TetR-DOZI system governs protein expression by regulating mRNA stability in response to anhydrous tetracycline (aTc). The conditional localization domain (CLD) directs the tagged *Ec*TilS protein to the parasitophorous vacuole upon *Shield1* administration; otherwise, it localizes to the apicoplast. This combined approach using aTc and *Shield1* offers enhanced control over *Ec*TilS-mCherry fusion protein levels. (H) Asynchronous *ectilS*$^{+}$Δ*pftilS* parasites resulted in a significant growth defect (two-way ANOVA, Sidak-Bonferroni method) under non-permissive conditions (absence of 0.5 μM aTc and presence of 0.5 μM *Shield1*) compared to parasites grown under permissive conditions (presence of 0.5 μM aTc and absence of 0.5 μM *Shield1*). Parasitemia was monitored daily for 8 days using flow cytometry. To prevent overgrowth, parasite cultures were diluted 1:10 on day 4. Data points represent the daily mean parasitemia ± SEM from two independent biological replicates, each with four technical replicates. (I) Representative epifluorescence microscopy of *ectilS*$^{+}$Δ*pftilS* parasites on day 4 (from panel H) shows an intact apicoplast under

permissive conditions. By contrast, multiple discrete vesicles suggesting a disrupted apicoplast were observed under non-permissive conditions. *Ec*TilS-mCherry fluorescence (magenta) is only visible under permissive conditions.

In (D) and (I), The *Ec*TilS protein is tagged with mCherry (magenta), api-SFG protein (green) labels the apicoplast, and nuclear DNA is stained with DAPI (blue). Each image depicts a field of 10 µm × 10 µm. In (B) and (E), DNA markers are in kilobases (kb).

Figure 6. Events leading to parasite death after of loss of TilS activity in the apicoplast

(A) TilS catalyzes lysidinylation of target $tRNA_{CAU}$ to modify wobble cytidine to lysidine post-transcriptionally. This modification ensures precise decoding of isoleucine codons during apicoplast protein translation, contributing to apicoplast maintenance and parasite survival. **(**B) Disruption of TilS activity leads to dysfunctional protein translation within the apicoplast. This is likely a consequence of impaired isoleucine decoding caused by the absence of the lysidine modification. The resulting disruption in apicoplast function ultimately culminates in parasite death.

Supplementary Figures and Tables

Supplementary Figure 1. Multiple sequence alignment (MSA) of TilS orthologs from *P. falciparum* (*Pf* TilS), *Synechocystis* sp. (*Sy* TilS), *Aquifex aeolicus* (*Aa* TilS), *Mycoplasma genitalium* (*Mg* TilS), *E. coli* (*Ec* TilS), *Geobacillus kaustophilus* (*Gk* TilS), and *Arabidopsis thaliana* (*At* RSY3). MSA output was visualized using Boxshade to highlight conserved residues. Amino acid residues and domains important for lysidinylation activity of TilS are depicted as in Figure 1(E).

Supplementary Figure 2. Pathogenic apicoplexans have TilS orthologs. TilS orthologs were identified in pathogenic apicomplexans using *P. falciparum* TilS as the query.

Supplementary Figure 3. The phylogenetic relationship among TilS orthologs. Phylogenetic analysis revealed a distant relationship between the TilS proteins of *P. falciparum* and *E. coli*. Bootstrap analyses (1000 replicates) were employed to assess the robustness of the branching patterns. The percentage of replicate trees in which the associated taxa clustered together is indicated adjacent to each branch. The phylogenetic tree is drawn to scale, with branch lengths representing the estimated number of substitutions per site.

Supplementary Figure 4. Uncropped image of immunoblot shown in Figure 4D. Immunoblot of saponin-isolated PfMev^{attB} (parental) and *ectilS*$^{+}$ parasite lysates with anti-mCherry antibodies (left panel) confirms expression of *Ec*TilS-mCherry fusion protein (expected molecular weight 91 kDa, black arrowhead). Anti-aldolase immunoblot shows relative loading levels (right panel). Protein markers are in kilodaltons (kDa).

Supplementary Figure 5. The phylogenetic relationship among methionine- and isoleucine-decoding tRNAs. Apicoplast encoded $tRNA_{CAU}$ are shown in blue font with PF3D7_API00600 (*pfal*_trnM-CAU2) sharing common ancestry with experimentally validated TilS substrate $tRNA^{Ile}_{CAU}$ from other species (in purple font). Bootstrap analyses (1000 replicates) were employed to assess the robustness of the branching patterns. The phylogenetic tree is drawn to

scale, with branch lengths representing the estimated number of substitutions per site. Refer to **Supplementary Table 3** for tRNA sequences.

Supplementary Figure 6. Comparison of secondary structures between *Escherichia coli* $tRNA^{Ile}_{CAU}$ and *Plasmodium falciparum* tRNAs from the apicoplast genome which are currently annotated as $tRNA^{Met}_{CAU}$. (A) *E. coli* $tRNA^{Ile}_{CAU}$. (B) PF3D7_API00600. (C) PF3D7_API06600 and PF3D7_API05000 (identical sequences due to gene duplication). In (A) and (B), the positive determinants for TilS binding are shown in magenta. In all panels, the dash (–) indicates canonical base pairing and the dot (.) indicates GU or UU base pairing.

Supplementary Figure 7. Sequence of codon-modified full-length *pftils* (in blue font) as synthesized. *AvrII* (CCTAGG) and *PspOMI* (GGGCCC) sites are underlined. The 3xV5 sequence is in magenta.

Supplementary Figure 8. Sequence of codon-modified N-terminally truncated *pftils* (in blue font) as synthesized. *AvrII* (CCTAGG) and *PspOMI* (GGGCCC) sites are underlined. The 3xV5 sequence is in magenta.

Supplementary Table 1. Primers used in this study. Restriction enzyme sites are underlined.

Supplementary Table 2. Proteins used for phylogenetic analysis presented in Supplementary Figure 3. [a]Uniprot ID, [b]PlasmoDB ID, [c]ToxoDB ID, [d]PiroplasmaDB ID.

Supplementary Table 3. tRNAs used for phylogenetic analysis presented in Supplementary Figure 5. Accession ID for apicoplast genome-encoded tRNAs are provided. *Pfal*, *Plasmodium falciparum*; *Tgon*, *Toxoplasma gondii*; *Eten*, *Eimeria tenella*; *Bmic*, *Babesia microti*; *Tpar*, *Theileria parva*; *Hmar*, *Haloarcula marismortui*; *Mmob*, *Mycoplasma mobile*; *Bsub*, *Bacillus subtilis*; *Ecol*, *Escherichia coli*; *Cpan*, *Cycas panzhihuaensis*; *Slyc*, *Solanum lycopersicum*; *Scer*, *Saccharomyces cerevisiae*.

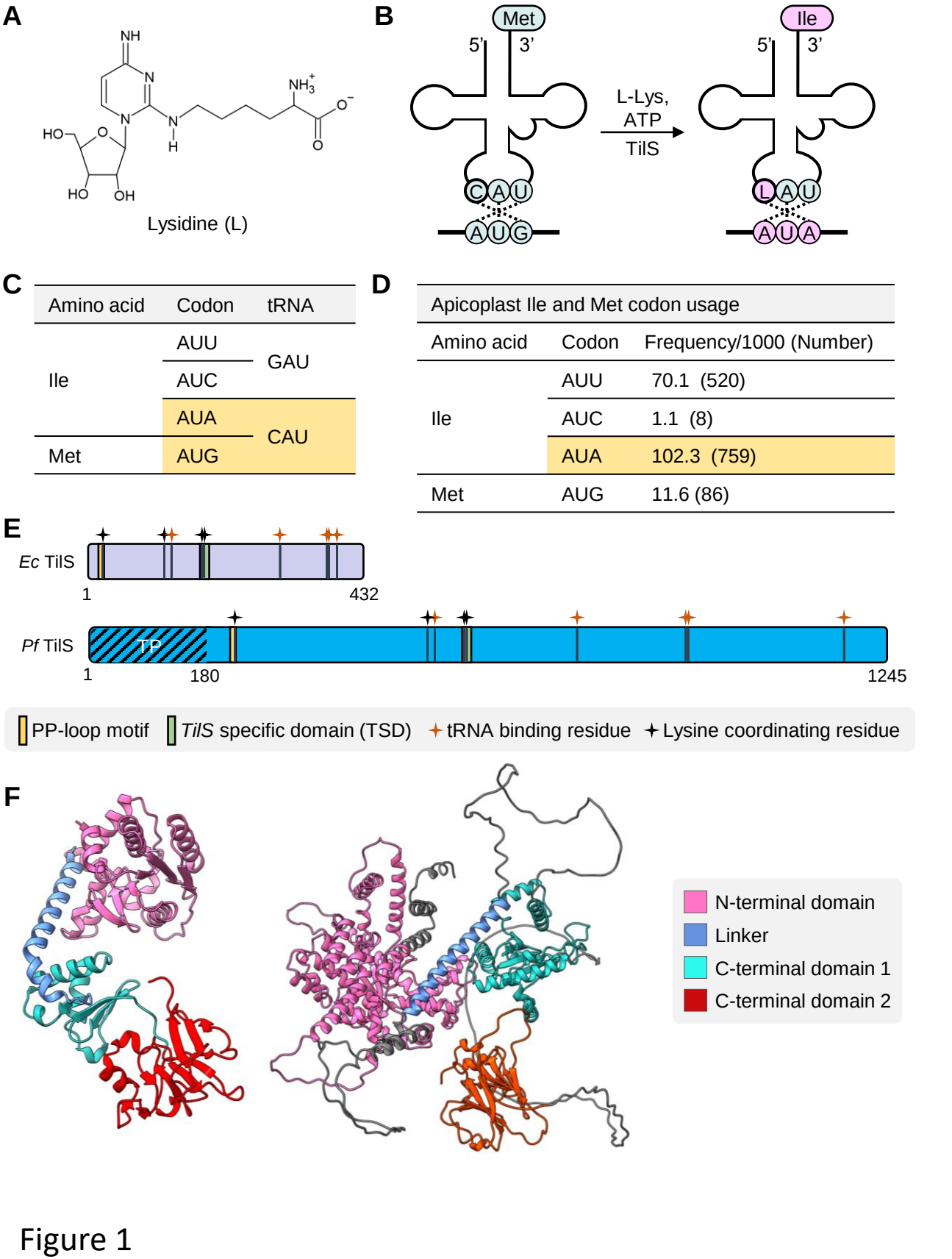
A
Lysidine (L)
B
Met
Ile
5'
3'
L-Lys,
ATP
TilS
C A U
A U G
L A U
A U A
C
Amino acid
Codon
tRNA
Ile
AUU
AUC
GAU
AUA
CAU
Met
AUG
D
Apicoplast Ile and Met codon usage
Amino acid
Codon
Frequency/1000 (Number)
Ile
AUU
70.1 (520)
AUC
1.1 (8)
AUA
102.3 (759)
Met
AUG
11.6 (86)
E
Ec TilS
1
432
Pf TilS
TP
1
180
1245
PP-loop motif
TilS specific domain (TSD)
tRNA binding residue
Lysine coordinating residue
F
N-terminal domain
Linker
C-terminal domain 1
C-terminal domain 2

Figure 1

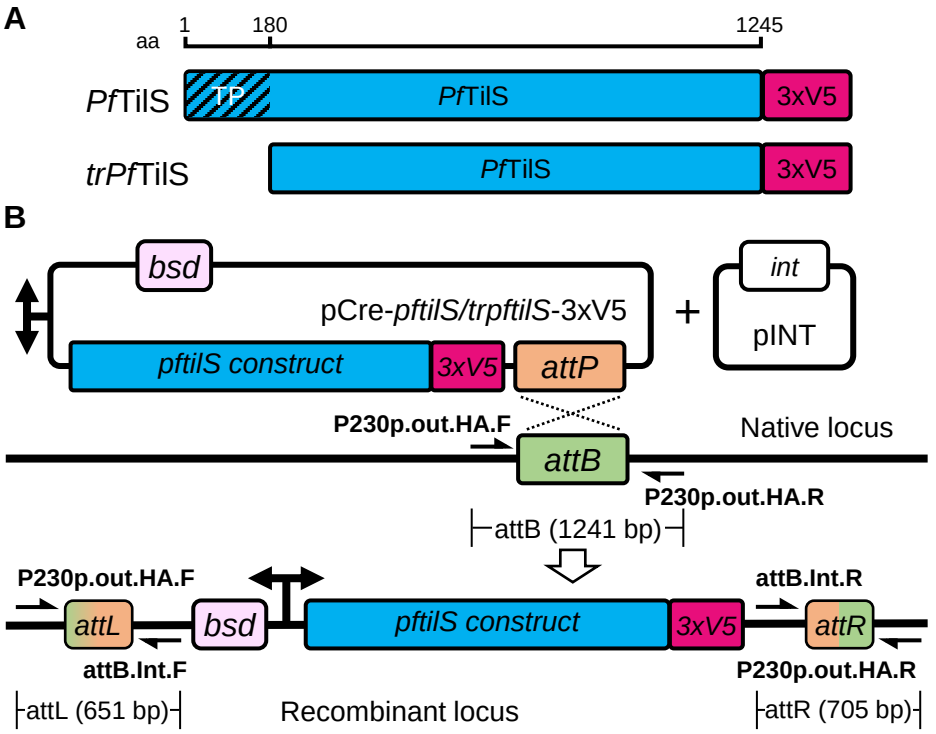
A
aa
1
180
1245
PfTilS
TP
PfTilS
3xV5
trPfTilS
PfTilS
3xV5
B
bsd
pCre-pftilS/trpftilS-3xV5
pftilS construct
3xV5
attP
+
int
pINT
P230p.out.HA.F
Native locus
attB
P230p.out.HA.R
attB (1241 bp)
P230p.out.HA.F
attL
bsd
pftilS construct
3xV5
attB.Int.R
attR
attB.Int.F
P230p.out.HA.R
attL (651 bp)
Recombinant locus
attR (705 bp)

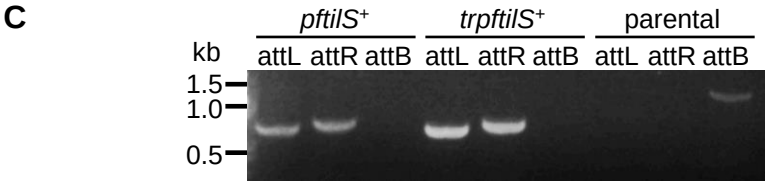
C
pftilS+
trpftilS+
parental
kb
attL attR attB attL attR attB attL attR attB
1.5
1.0
0.5

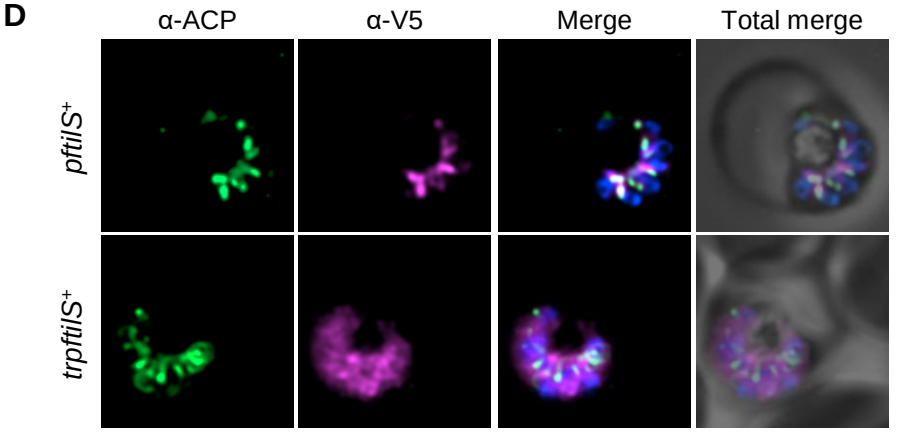
D
α-ACP
α-V5
Merge
Total merge
pftilS+
trpftilS+

Figure 2

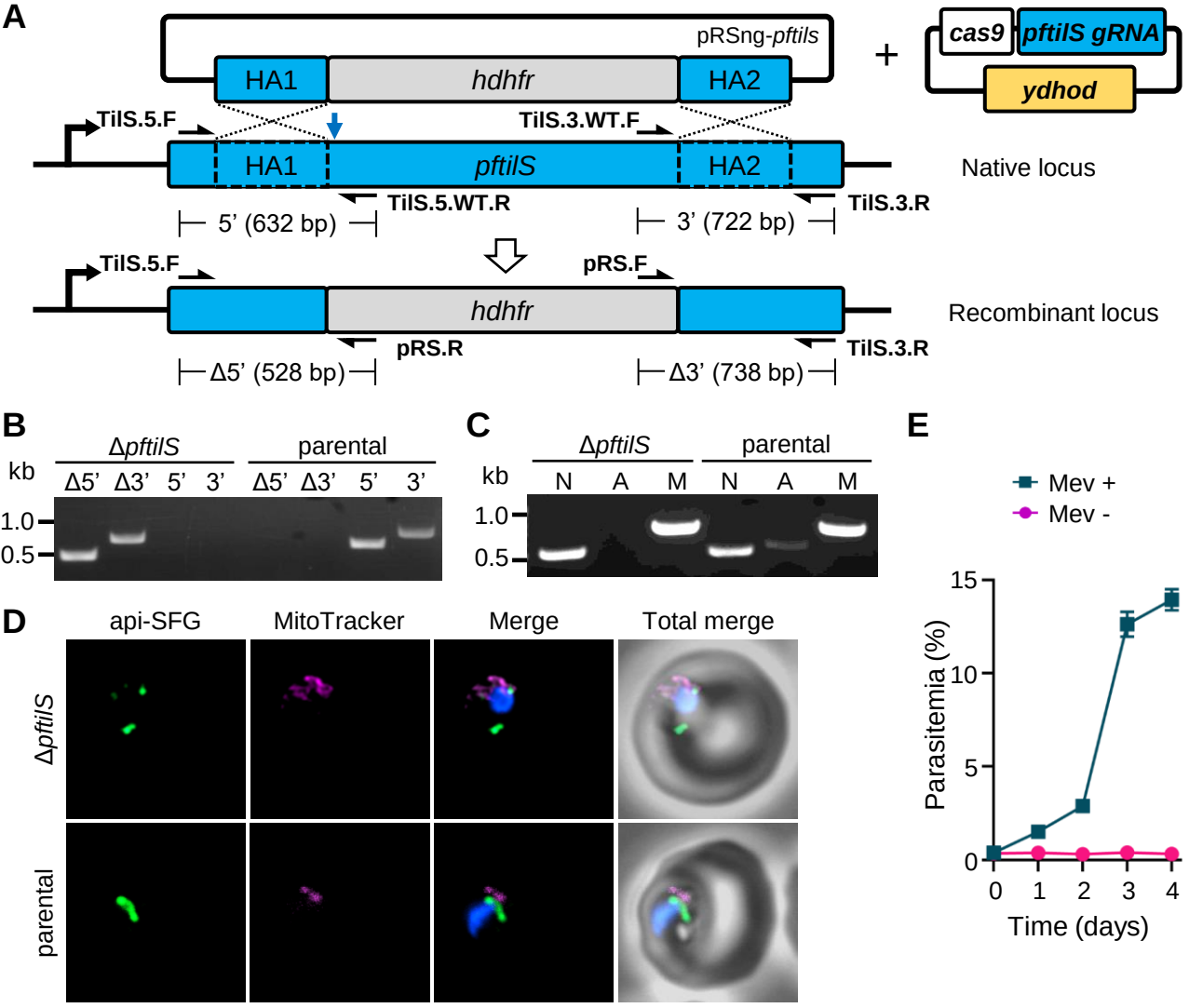
A
pRSng-pftilS
HA1
hdhfr
HA2
cas9
pftilS gRNA
ydhod
TilS.5.F
TilS.3.WT.F
HA1
pftilS
HA2
Native locus
TilS.5.WT.R
TilS.3.R
5' (632 bp)
3' (722 bp)
TilS.5.F
pRS.F
hdhfr
Recombinant locus
pRS.R
TilS.3.R
Δ5' (528 bp)
Δ3' (738 bp)
B
ΔpftilS
parental
kb
Δ5' Δ3' 5' 3' Δ5' Δ3' 5' 3'
1.0
0.5
C
ΔpftilS
parental
kb
N A M N A M
1.0
0.5
D
api-SFG
MitoTracker
Merge
Total merge
ΔpftilS
parental
E
Mev +
Mev -
Parasitemia (%)
15
10
5
0
0 1 2 3 4
Time (days)

Figure 3

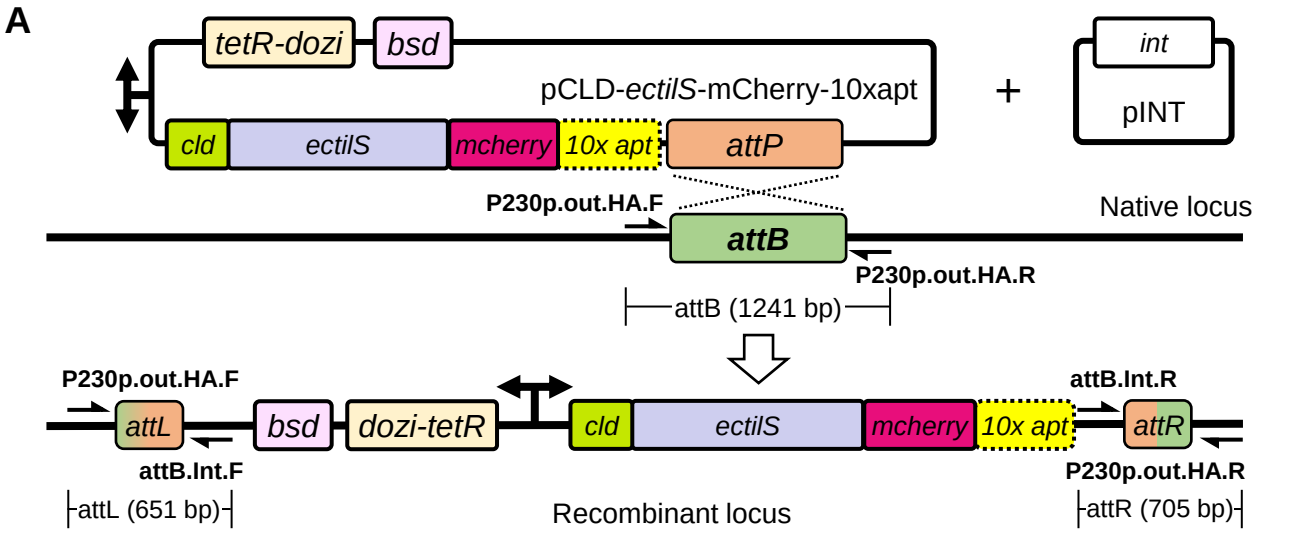
A
tetR-dozi
bsd
pCLD-ectilS-mCherry-10xapt
cld
ectilS
mcherry
10x apt
attP
int
pINT
P230p.out.HA.F
attB
Native locus
P230p.out.HA.R
attB (1241 bp)
P230p.out.HA.F
attL
bsd
dozi-tetR
cld
ectilS
mcherry
10x apt
attB.Int.R
attR
attB.Int.F
P230p.out.HA.R
attL (651 bp)
Recombinant locus
attR (705 bp)

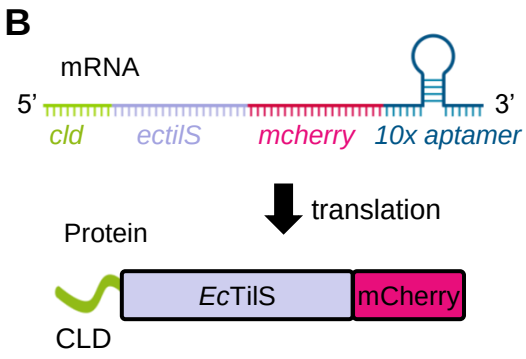
B
mRNA
5'
3'
cld
ectilS
mcherry
10x aptamer
translation
Protein
EcTilS
mCherry
CLD

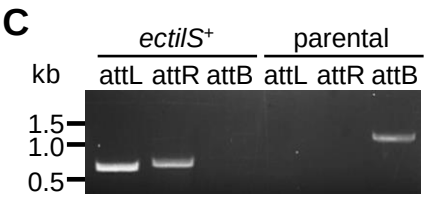
C
ectilS+
parental
kb
attL attR attB attL attR attB
1.5
1.0
0.5

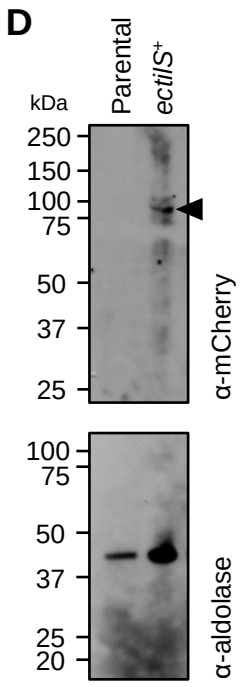
D
Parental
ectilS+
kDa
250
150
100
75
50
37
25
α-mCherry
100
75
50
37
25
20
α-aldolase

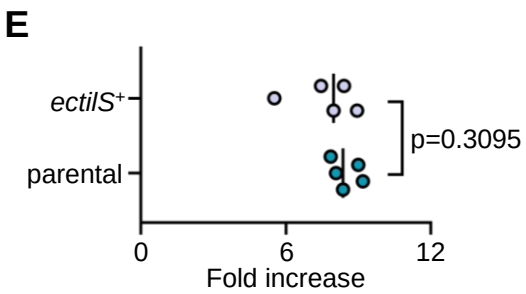
E
ectilS+
parental
p=0.3095
0
6
12
Fold increase

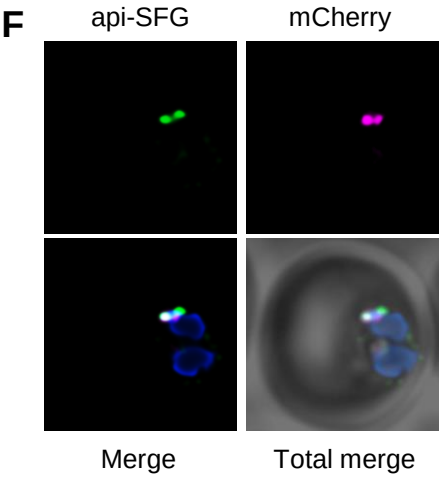
F
api-SFG
mCherry
Merge
Total merge

Figure 4

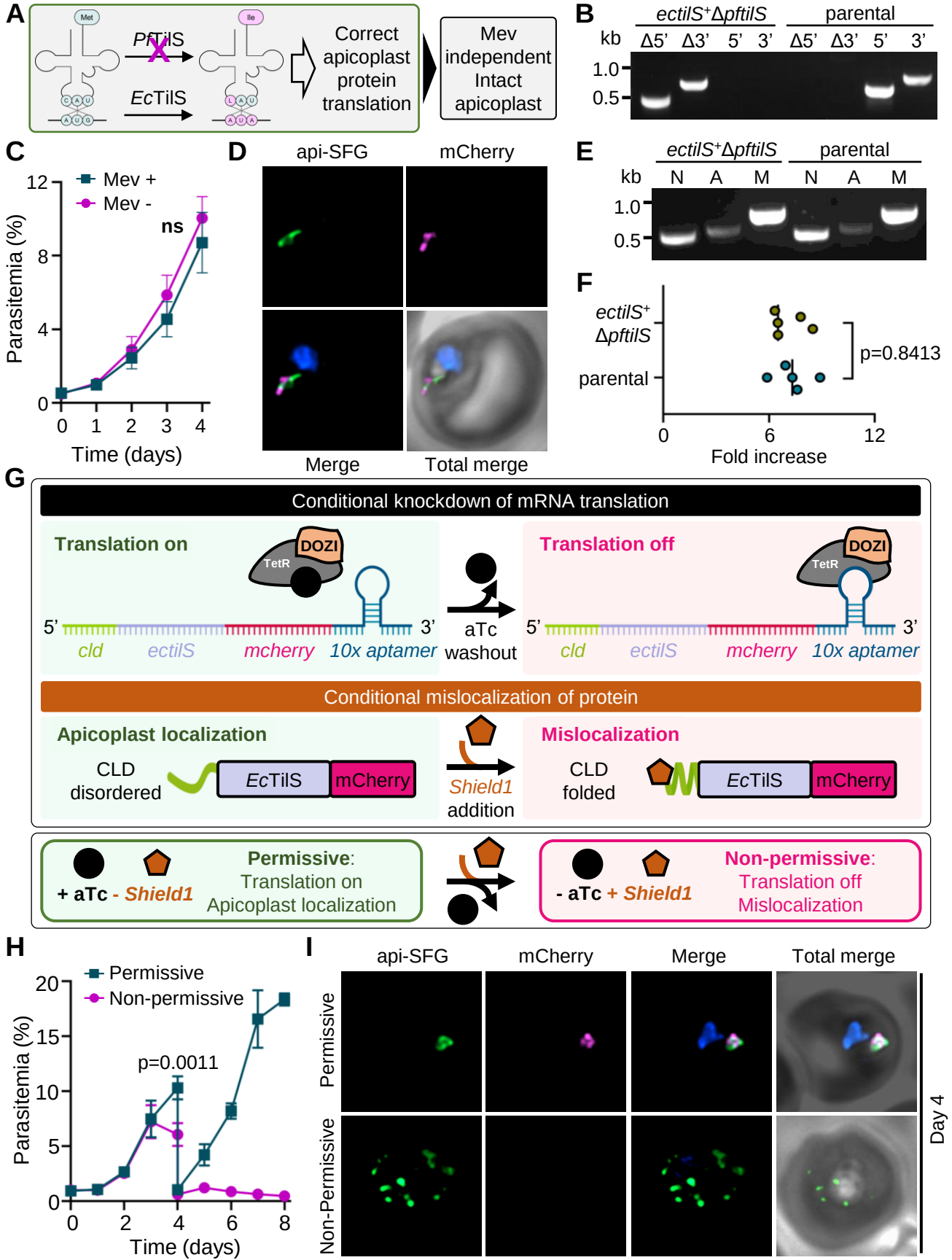
A
Met
Ile
PfTilS
EcTilS
Correct apicoplast protein translation
Mev independent Intact apicoplast
B
ectilS+ΔpftilS
parental
kb
Δ5' Δ3' 5' 3' Δ5' Δ3' 5' 3'
1.0
0.5
C
Mev +
Mev -
ns
Parasitemia (%)
Time (days)
D
api-SFG
mCherry
Merge
Total merge
E
ectilS+ΔpftilS
parental
kb
N A M N A M
1.0
0.5
F
ectilS+ ΔpftilS
parental
p=0.8413
Fold increase
G
Conditional knockdown of mRNA translation
Translation on
DOZI
TetR
5'
3'
cld
ectilS
mcherry
10x aptamer
aTc washout
Translation off
Conditional mislocalization of protein
Apicoplast localization
CLD disordered
EcTilS
mCherry
Shield1 addition
Mislocalization
CLD folded
+ aTc - Shield1
Permissive: Translation on Apicoplast localization
- aTc + Shield1
Non-permissive: Translation off Mislocalization
H
Permissive
Non-permissive
p=0.0011
Parasitemia (%)
Time (days)
I
api-SFG
mCherry
Merge
Total merge
Permissive
Non-Permissive
Day 4

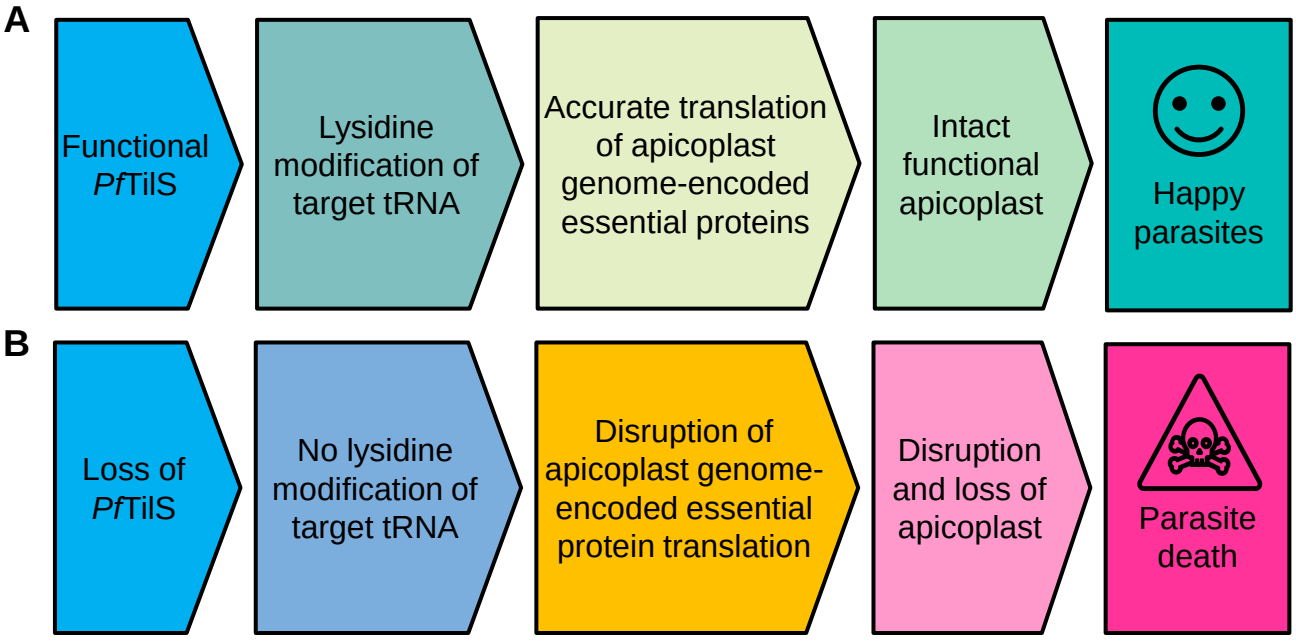
A
Functional *Pf*TilS
Lysidine modification of target tRNA
Accurate translation of apicoplast genome-encoded essential proteins
Intact functional apicoplast
Happy parasites
B
Loss of *Pf*TilS
No lysidine modification of target tRNA
Disruption of apicoplast genome-encoded essential protein translation
Disruption and loss of apicoplast
Parasite death

Figure 6

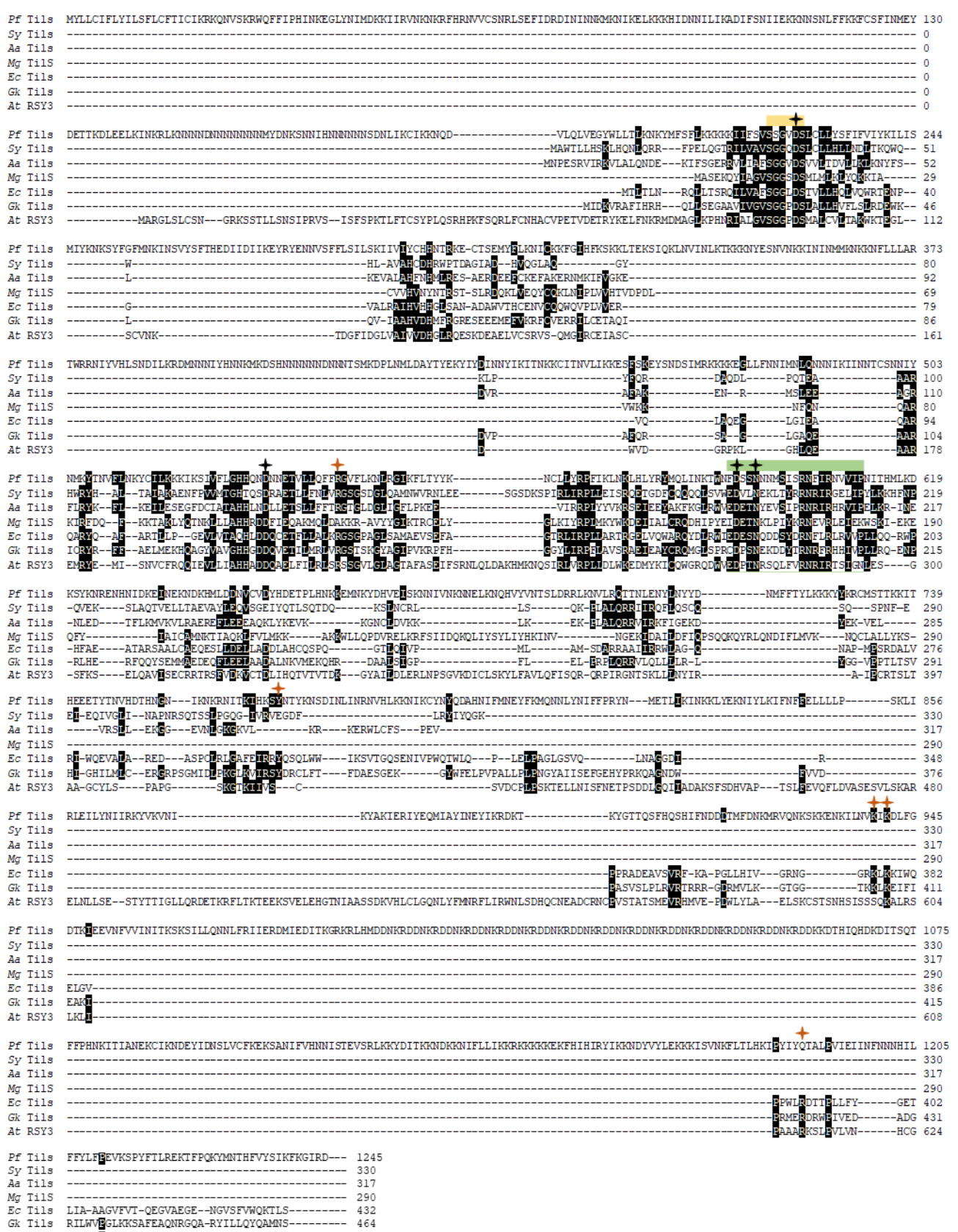

Supplementary Figure 1

Apicomplexans	Gene ID	Identity to Pf TilS	E-value	Experimental localization
Toxoplasma gondii	TGME49_215100	30%	1e-8	Apicoplast*
Eimeria tenella	ETH2_0718500	23%	0.025	N.D.
Neospora caninum	NCLIV_052110	30%	8e-10	N.D.
Babesia microti	BMR1_01G01110	39%	1e-11	N.D.
Theileria annulata	TA03600	30%	2e-4	N.D.

* Identified in the apicoplast fraction from *T. gondii* via hyperLOPIT
N.D., not determined

Supplementary Figure 2

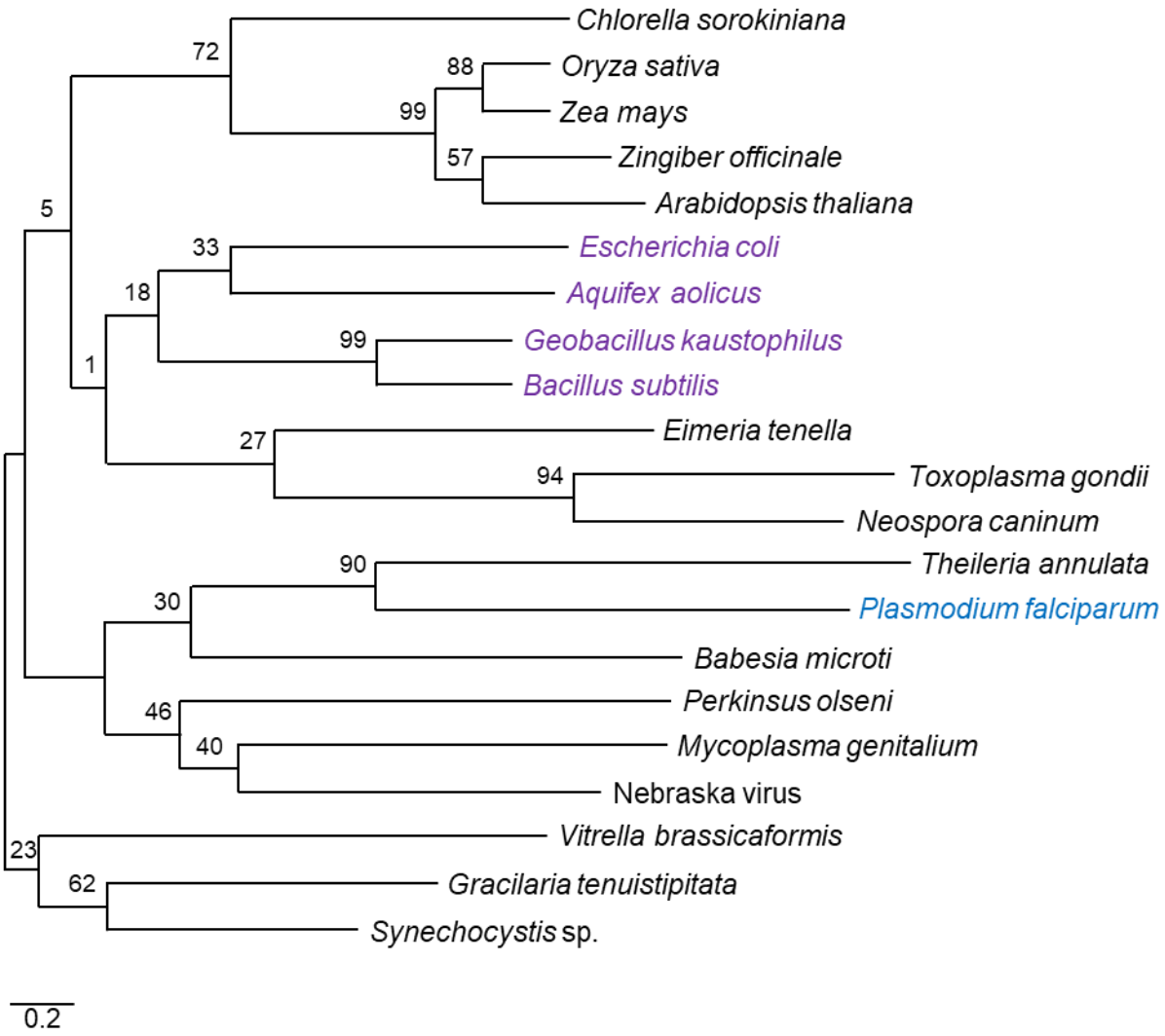

Supplementary figure 3

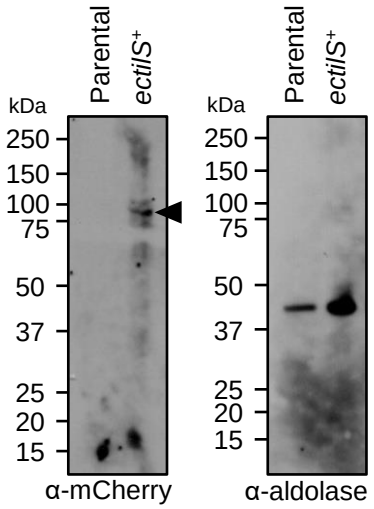

Supplementary Figure 4

Supplementary Figure 5

A

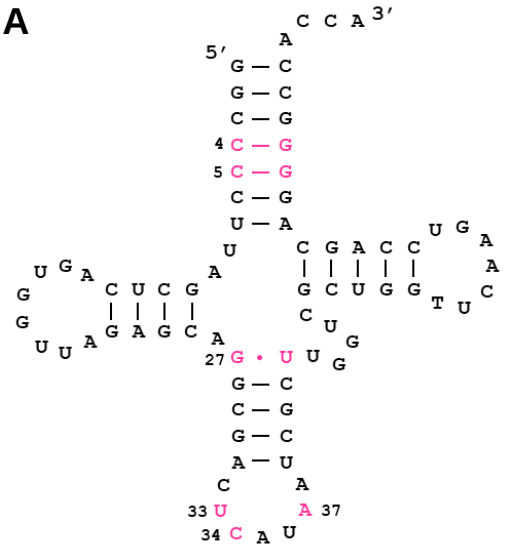

E. coli $tRNA_{CAU}^{Ile}$

B

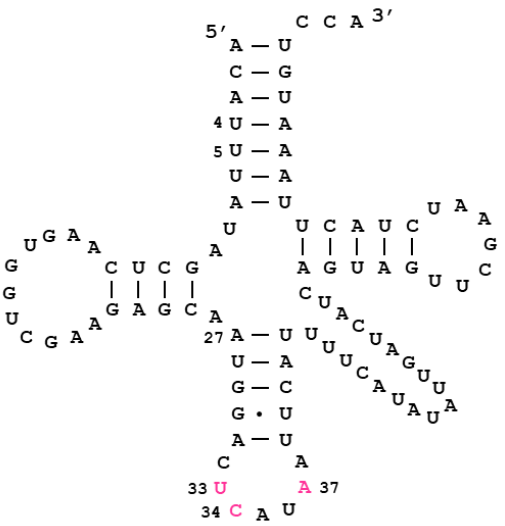

P. falciparum $tRNA_{CAU}2$
PF3D7_API00600

C

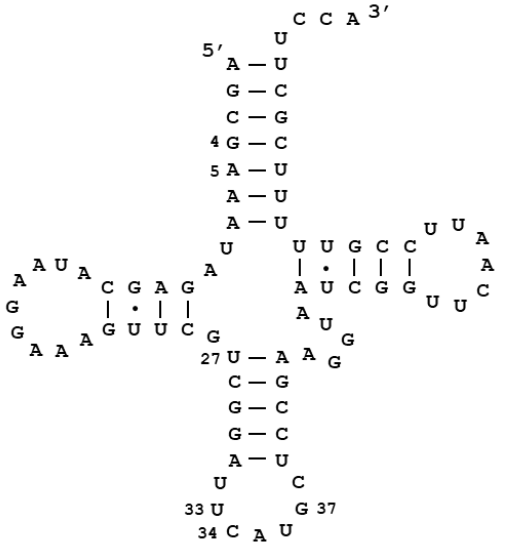

P. falciparum $tRNA_{CAU}1$
PF3D7_API06600

P. falciparum $tRNA_{CAU}3$
PF3D7_API05000

Supplementary Figure 6

CCTAGGATGTACCTGCTGTGCATTTTCCTGTATATCTTGAGCTTTTTATGTTTTACAATTTGTATTAAACGTAAACAG
AACGTCTCGAAGCGTTGGCAGTTTTTCATTCCGCATATTAACAAGGAAGGCCTTTACAATATCATGGATAAGAAAAT
CATCCGGGTCAACAAAAACAAACGGTTCCATCGTAACGTTGTATGCAGCAACCGGCTGAGTGAATTCATCGATCGC
GATATCAACATTAACAACAAGATGAAGAATATCAAGGAACTGAAAAAAAAACACATTGATAACAACATTTTGATTAAA
GCAGACATTTTCAGCAACATAATCGAGAAAAAAAACAATTCAAACTTATTTTTTAAAAAATTTTGCTCTTTTATTAACA
TGGAATATGACGAAACCACCAAAGATTTAGAAGAGTTAAAAATCAACAAACGATTGAAAAACAATAACAATGATAAT
AACAACAATAACAACAACAACATGTATGATAACAAAAGCAATAATATTCATAACAACAACAATAACAATAGCGATAAT
TTGATTAAATGTATCAAAAAGAATCAGGATGTGCTGCAGTTGGTAGAAGGATACTGGCTGTTAACGCTGAAAAACA
AATATATGTTTTCTTTTCTGAAAAAAAAGAAAAAAATTATCTTCAGCGTGTCAAGTGGGGTGGACTCTTTGTGCCTTC
TTTATAGCTTCATCTTTGTTATCTATAAAATTCTGATCAGCATGATTTACAAAAATAAAAGTTATTTTGGCTTTATGAA
TAAAATCAACAGCGTGTATAGCTTTACTCATGAAGATATTATTGATATCATCAAAGAATACCGTTATGAAAACAATGT
CAGCTTCTTTCTGTCGATCCTGAGCAAAATTATCGTGATTTACTGTCATCATAATACCCGTAAAGAATGTACCTCAG
AAATGTATTTTCTTAAAAACATTTGCAAAAAATTCGGTATCCACTTTAAATCCAAAAAACTGACGGAAAAGAGTATTC
AGAAACTGAATGTAATAAACTTAAAAACGAAAAAGAAAAATTACGAAAGCAATGTGAATAAGAAAATTAATATTAACA
TGATGAAGAATAAAAAAAATTTCCTGCTGCTAGCACGAACCTGGCGTCGTAACATCTACGTGCACCTCTCCAACGA
TATTTTGAAACGGGACATGAACAACAATATTTATCACAACAACAAAATGAAAGATTCCCATAACAACAACAACAATAA
CGATAATAACAACACGAGCATGAAGGACCCCCTGAATATGTTAGATGCTTATACCTACGAAAAATATATTTACGATA
TTAACAATTATATCAAAATCACCAACAAAAAATGCATCACCAACGTCCTGATTAAGAAAGAATCATTCAGTAAGGAG
TACTCCAACGATTCGATCATGCGCAAGAAGAAAAAGGAAGGTCTGCTTTTCAATAATATTATGAACCTGCAGAATAA
TAACATTAAAATTATCAACAACACTTGCAGCAATAATATTTACAATATGAAATATACTAATGTTTTTCTGAACAAATAT
TGCATCCTGAAAAAAAAGATTAAATCAATCGTGTTCCTCGGCCACCACCAGAACGACAACAACGAAACGGTGCTGC
TTCAGTTCTTCCGTGGTGTTTTTTTAAAAAACCTGCGCGGCATTAAATTTCTCACCTACTATAAAAATTGTCTGCTGT
ATCGTCCGTTCATCAAACTGAACAAACTCCATTTGTATCGCTACATGCAGCTTATCAACAAAACTTGGAATTTCGAT
TCCTCTAACAACAATATGTCTATTTCGCGTAACTTCATCCGCAATGTGGTGATCCCAAACATAACCCATATGTTGAA
AGATAAAAGCTATAAAAATCGTGAGAACCACAATATTGACAAAGAGATTAATGAGAAGAATGATAAGCACATGCTGG
ATGATAACGTGTGCGTTGATTACCATGATGAAACACCCCTTCATAATAAGAAAGAAATGAATAAATATGATCATGTC
GAAATTTCGAAAAATAACATCGTTAACAAAAACAATGAACTGAAAAACCAGCATGTATATGTCAATACCTCTCTGGA
TCGTCGCCTGAAAAACGTTCTGCGCCAGACCACGAACCTGGAAAATTACCTGAATTATTATGACAATATGTTCTTTA
CCTATCTGAAAAAGAAATATTACAAACGCTGCATGTCAACCACAAAAAAGATTACGCATGAAGAAGAGACGTACACT
AACGTCCATGATACCCATAACGGCAACATCAAAAATAAACGCAACATCACCAAAATTCACAAAAGTTATAACACCTA
TAAAAACTCCGATATAAATTTAATCAATCGTAACGTGCATTTGAAAAAAAACATTAAATGCTACAACTATCAGGATGC
GCATAACATCTTTATGAACGAATACTTTAAAATGCAAAACAATCTGTATAACATCTTTTTCCCGCGTTACAACATGGA
AACACTGATCAAAATTAACAAAAAACTGTACGAGAAAAACATTTACCTGAAAATTTTTAACTTCTTCGAACTCCTGCT
GCTGCCTTCTAAACTCATCCGCCTCGAAATTCTGTATAACATCATCCGTAAATATGTCAAGGTAAACATTAAATATG
CCAAGATAGAACGGATTTATGAACAAATGATTGCGTACATTAATGAATATATCAAACGTGATAAAACAAAATACGGT
ACCACGCAATCGTTTCATCAATCGCATATATTCAACGATGATGATACTATGTTCGACAATAAAATGCGTGTTCAGAA
TAAAAGCAAAAAGGAAAATAAAATCCTGAACGTGAAAATTAAGGATTTGTTTGGGGATACCAAAATTGAGGAGGTG
AACTTTGTGGTGATTAATATTACTAAAAGTAAGTCAATCCTTCTCCAAAACAACCTGTTCCGGATTATTGAACGCGAT
ATGATCGAAGATATTACCAAAGGACGCAAACGCCTCCACATGGACGATAACAAACGCGACGATAATAAACGCGAC
GATAACAAACGCGACGATAACAAACGCGACGATAACAAACGGGACGATAATAAACGCGACGATAACAAACGTGAC
GATAATAAACGTGACGATAATAAACGCGACGATAACAAACGTGACGACAACAAACGGGACGATAACAAACGGGAC
GATAATAAACGGGATGATAAAAAAGATACCCACATTCAGCACGATAAGGATATTACATCACAAACCTTTTTCCCTCA
CAACAAAATTACAATTGCCAACGAGAAATGTATTAAAAACGATGAATACATTGACAACAGCCTGGTCTGTTTTAAAG
AAAAAAGCGCCAATATCTTTGTCCATAATAATATTTCCACGGAGGTGTCTCGCCTGAAAAAATATGATATCACGAAA
AAGAACGATAAAAAGAACATCTTTCTTCTAATCAAAAAGCGGAAAAAAAAAAAAAAAGAAAAATTTCACATTCACATT
CGATACATTAAAAAAAATGATTATGTTTATCTGGAAAAAAAAAAAATCTCCGTTAATAAATTTCTGACCCTTCACAAG
ATCCCGTATATTTATCAGACCGCGCTGCCGGTTATTGAAATTATCAATTTTAATAATAACCATATTCTGTTTTTTTATT
TGTTCCCGGAAGTGAAAAGCCCGTATTTCACTCTGCGAGAAAAAACGTTTCCACAAAAATATATGAATACACATTTT
GTTTATAGTATCAAATTCAAGGGGATCCGTGACCGTACGGACGTCGGAAAACCAATACCAAATCCTTTGTTAGGTT
TAGACAGTACAGGAGGTAAACCTATACCTAATCCTTTATTGGGTCTTGATTCAACTGGTGGAAAACCTATTCCAAAT
CCATTATTAGGATTAGATTCTACATAAGGGCCC

Supplementary Figure 7

CCTAGGATGATTAAATGTATCAAAAAGAATCAGGATGTGCTGCAGTTGGTAGAAGGATACTGGCTGTTAACGCTGA
AAAACAAATATATGTTTTCTTTTCTGAAAAAAAAGAAAAAAATTATCTTCAGCGTGTCAAGTGGGGTGGACTCTTTGT
GCCTTCTTTATAGCTTCATCTTTGTTATCTATAAAATTCTGATCAGCATGATTTACAAAAATAAAAGTTATTTTGGCTT
TATGAATAAAATCAACAGCGTGTATAGCTTTACTCATGAAGATATTATTGATATCATCAAAGAATACCGTTATGAAAA
CAATGTCAGCTTCTTTCTGTCGATCCTGAGCAAAATTATCGTGATTTACTGTCATCATAATACCCGTAAAGAATGTA
CCTCAGAAATGTATTTTCTTAAAAACATTTGCAAAAAATTCGGTATCCACTTTAAATCCAAAAAACTGACGGAAAAGA
GTATTCAGAAACTGAATGTAATAAACTTAAAAACGAAAAAGAAAAATTACGAAAGCAATGTGAATAAGAAAATTAATA
TTAACATGATGAAGAATAAAAAAAATTTCCTGCTGCTAGCACGAACCTGGCGTCGTAACATCTACGTGCACCTCTC
CAACGATATTTTGAAACGGGACATGAACAACAATATTTATCACAACAACAAAATGAAAGATTCCCATAACAACAACA
ACAATAACGATAATAACAACACGAGCATGAAGGACCCCCTGAATATGTTAGATGCTTATACCTACGAAAAATATATT
TACGATATTAACAATTATATCAAAATCACCAACAAAAAATGCATCACCAACGTCCTGATTAAGAAAGAATCATTCAGT
AAGGAGTACTCCAACGATTCGATCATGCGCAAGAAGAAAAAGGAAGGTCTGCTTTTCAATAATATTATGAACCTGC
AGAATAATAACATTAAAATTATCAACAACACTTGCAGCAATAATATTTACAATATGAAATATACTAATGTTTTTCTGAA
CAAATATTGCATCCTGAAAAAAAAGATTAAATCAATCGTGTTCCTCGGCCACCACCAGAACGACAACAACGAAACG
GTGCTGCTTCAGTTCTTCCGTGGTGTTTTTTTAAAAAACCTGCGCGGCATTAAATTTCTCACCTACTATAAAAATTGT
CTGCTGTATCGTCCGTTCATCAAACTGAACAAACTCCATTTGTATCGCTACATGCAGCTTATCAACAAAACTTGGAA
TTTCGATTCCTCTAACAACAATATGTCTATTTCGCGTAACTTCATCCGCAATGTGGTGATCCCAAACATAACCCATAT
GTTGAAAGATAAAAGCTATAAAAATCGTGAGAACCACAATATTGACAAAGAGATTAATGAGAAGAATGATAAGCACA
TGCTGGATGATAACGTGTGCGTTGATTACCATGATGAAACACCCCTTCATAATAAGAAAGAAATGAATAAATATGAT
CATGTCGAAATTTCGAAAAATAACATCGTTAACAAAAACAATGAACTGAAAAACCAGCATGTATATGTCAATACCTCT
CTGGATCGTCGCCTGAAAAACGTTCTGCGCCAGACCACGAACCTGGAAAATTACCTGAATTATTATGACAATATGT
TCTTTACCTATCTGAAAAAGAAATATTACAAACGCTGCATGTCAACCACAAAAAAGATTACGCATGAAGAAGAGACG
TACACTAACGTCCATGATACCCATAACGGCAACATCAAAAATAAACGCAACATCACCAAAATTCACAAAAGTTATAA
CACCTATAAAAACTCCGATATAAATTTAATCAATCGTAACGTGCATTTGAAAAAAAACATTAAATGCTACAACTATCA
GGATGCGCATAACATCTTTATGAACGAATACTTTAAAATGCAAAACAATCTGTATAACATCTTTTTCCCGCGTTACAA
CATGGAAACACTGATCAAAATTAACAAAAAACTGTACGAGAAAAACATTTACCTGAAAATTTTTAACTTCTTCGAACT
CCTGCTGCTGCCTTCTAAACTCATCCGCCTCGAAATTCTGTATAACATCATCCGTAAATATGTCAAGGTAAACATTA
AATATGCCAAGATAGAACGGATTTATGAACAAATGATTGCGTACATTAATGAATATATCAAACGTGATAAAACAAAAT
ACGGTACCACGCAATCGTTTCATCAATCGCATATATTCAACGATGATGATACTATGTTCGACAATAAAATGCGTGTT
CAGAATAAAAGCAAAAAGGAAAATAAAATCCTGAACGTGAAAATTAAGGATTTGTTTGGGGATACCAAAATTGAGGA
GGTGAACTTTGTGGTGATTAATATTACTAAAAGTAAGTCAATCCTTCTCCAAAACAACCTGTTCCGGATTATTGAAC
GCGATATGATCGAAGATATTACCAAAGGACGCAAACGCCTCCACATGGACGATAACAAACGCGACGATAATAAAC
GCGACGATAACAAACGCGACGATAACAAACGCGACGATAACAAACGGGACGATAATAAACGCGACGATAACAAAC
GTGACGATAATAAACGTGACGATAATAAACGCGACGATAACAAACGTGACGACAACAAACGGGACGATAACAAAC
GGGACGATAATAAACGGGATGATAAAAAAGATACCCACATTCAGCACGATAAGGATATTACATCACAAACCTTTTTC
CCTCACAACAAAATTACAATTGCCAACGAGAAATGTATTAAAAACGATGAATACATTGACAACAGCCTGGTCTGTTT
TAAAGAAAAAAGCGCCAATATCTTTGTCCATAATAATATTTCCACGGAGGTGTCTCGCCTGAAAAAATATGATATCA
CGAAAAAGAACGATAAAAAGAACATCTTTCTTCTAATCAAAAAGCGGAAAAAAAAAAAAAAAGAAAAATTTCACATTC
ACATTCGATACATTAAAAAAAATGATTATGTTTATCTGGAAAAAAAAAAAATCTCCGTTAATAAATTTCTGACCCTTCA
CAAGATCCCGTATATTTATCAGACCGCGCTGCCGGTTATTGAAATTATCAATTTTAATAATAACCATATTCTGTTTTT
TTATTTGTTCCCGGAAGTGAAAAGCCCGTATTTCACTCTGCGAGAAAAAACGTTTCCACAAAAATATATGAATACAC
ATTTTGTTTATAGTATCAAATTCAAGGGGATCCGTGACCGTACGGACGTCGGAAAACCAATACCAAATCCTTTGTTA
GGTTTAGACAGTACAGGAGGTAAACCTATACCTAATCCTTTATTGGGTCTTGATTCAACTGGTGGAAAACCTATTCC
AAATCCATTATTAGGATTAGATTCTACATAAGGGCCC

Supplementary Figure 8